Title

SARM1 depletion rescues NMNAT1 dependent photoreceptor cell death and retinal degeneration.

Authors

Yo Sasaki [1]

Hiroki Kakita [1,6]

Shunsuke Kubota [2]

Abdoulaye Sene [2]

Tae Jun Lee [2]

Norimitsu Ban [2]

Zhenyu Dong [2]

Joseph B. Lin [2]

Sanford L. Boye [5]

Aaron DiAntonio [3,7]

Shannon E. Boye [5]

Rajendra S. Apte [2,3,4]

Jeffrey Milbrandt [1,7]

[1] Department of Genetics, Washington University School of Medicine, St. Louis, MO 63110

[2] Department of Ophthalmology and Visual Sciences, Washington University School of Medicine, St. Louis, MO 63110

[3] Department of Developmental Biology, Washington University School of Medicine, St. Louis, 63110

[4] Department of Medicine, Washington University School of Medicine, St. Louis, MO 63110

[5] Department of Ophthalmology, University of Florida, Gainesville, FL, 32610

[6] Department of Perinatal and Neonatal Medicine, Aichi Medical University, Aichi 480-1195, Japan

[7] Needleman Center for Neurometabolism and Axonal Therapeutics

Address Correspondence to: apte@wustl.edu and sasaki@wustl.edu

Abstract

Leber congenital amaurosis type 9 (LCA9) is an autosomal recessive, early onset retinal neurodegenerative disease caused by mutations in the gene encoding the nuclear NAD^+ synthesis enzyme NMNAT1. Despite the ubiquitous expression of NMNAT1 and its role in NAD^+ homeostasis, LCA9 patients do not manifest pathologies other than retinal degeneration. To investigate the mechanism of degeneration, we examined retinas of developing and adult mice with conditional or tissue-specific NMNAT1 loss. Widespread NMNAT1 depletion in adult mice resulted in loss of photoreceptors, indicating these cells are exquisitely vulnerable to NMNAT1 loss. NMNAT1 is required within the photoreceptor, as conditional deletion of NMNAT1 in photoreceptors but not retinal pigment epithelial cells is sufficient to cause photoreceptor neurodegeneration and vision loss. Moreover, delivery of NMNAT1 into eyes of adult mice lacking NMNAT1 using a modified AAV8 vector containing a photoreceptor-specific promoter rescued the retinal degeneration phenotype and partially restored vision. Finally, we defined the molecular mechanism driving photoreceptor cell death. Loss of NMNAT1 activates SARM1, an inducible NADase best known as the central executioner of axon degeneration. SARM1 is required for the photoreceptor death and vision loss that occurs following NMNAT1 deletion. This surprising finding demonstrates that the essential function of NMNAT1 in photoreceptors is to inhibit SARM1, and establishes a commonality of mechanism between axonal degeneration and photoreceptor neurodegeneration. These results define a novel SARM1-dependent photoreceptor cell death pathway that is active in the setting of dysregulated NAD^+ metabolism and identifies SARM1 as a therapeutic candidate for the treatment of retinal degeneration.

Introduction

Leber congenital amaurosis (LCA) is a retinal degenerative disease characterized by childhood onset and severe loss of vision. LCA is the most common cause of blindness in children and about 70% of LCA cases are associated with mutations in genes related to the visual cycle, cGMP production, ciliogenesis, or transcription. Recently, more than thirty mutations in the nuclear NAD^+ biosynthetic enzyme NMNAT1 were identified in patients with autosomal recessive LCA type 9 [1-6]. Despite the ubiquitous expression of this key NAD^+ biosynthesis enzyme, LCA9 patients have no other systemic deficits outside the retina. In many cases, LCA9 associated mutant NMNAT1 proteins retain enzymatic activity and other biochemical functions, but appear to be less stable under conditions associated with cell stress [7]. While it is clear that NAD^+ deficiency in the retina is an early feature of retinal degenerative disorders in mice [8,9], it is not known which cell types and biological pathways are primarily affected in LCA9.

NMNAT1 plays important roles in diverse retinal functions. Overexpression of NMNAT1 in mouse retinal ganglion cells (RGCs) robustly protects against ischemic and glaucomatous loss of the axon and soma [10], while conditional ablation in the developing mouse retina causes severe retinal dystrophy and loss of retinal function [11,12]. Mice harboring *Nmnat1* mutations (V9M and D243G) exhibit severe retinal degeneration while the most common LCA9 mutation (E257K), which is not fully penetrant [13], induces a milder retinal degeneration phenotype [11,14]. In retinal explants, NMNAT1 promotes the survival of mouse retinal progenitor cells [15]. The requirement for NMNAT in retina is evolutionarily conserved, as the *Drosophila* NMNAT isoform, dNMNAT, is required for the survival of photoreceptor cells after exposure to intense light [16,17].

The selective loss of photoreceptor cells in LCA9 suggests the survival and function of these cells are extremely sensitive to deranged NAD^+ metabolism in these cells. Indeed, many of the enzymes involved in photoreceptor function are dependent on NAD^+ as a cofactor, and for some of these proteins mutations in their corresponding genes lead to blindness. These include variants in the NAD^+ or NADPH dependent retinal dehydrogenases like RDH12 that cause LCA13 [18] and the GTP synthesis enzyme IMPDH1 that causes retinitis pigmentosa [19,20].

SIRT3, the mitochondrial NAD^+-dependent deacetylase is also important for photoreceptor homeostasis [9,21]. Together, these observations highlight the importance of cytosolic NAD^+ dependent pathways in retinal function [9,22]; however, the molecular roles of nuclear NAD^+ and NMNAT1 in the retina are largely unknown.

Multiple enzymatic pathways utilizing distinct metabolic precursors participate in NAD^+ biosynthesis [23]. However, in each case, these pathways converge at an NMNAT-dependent step that generates either NAD^+ or its deamidated form NaAD from the precursor NMN or NaMN. Among the three mammalian NMNAT isoforms, NMNAT1 is the only enzyme localized to the nucleus [24]. However, in photoreceptors NMNAT1 also localizes near the cilia basal body [11], consistent with an additional, extra-nuclear role of NMNAT1 in photoreceptor cells. This is of particular interest because engineered non-nuclear variants of enzymatically-active NMNAT1 can potently inhibit pathological axon degeneration, which is commonly observed in the early stages of many neurodegenerative disorders [25-27]. When NMNAT1 is present in the axon, it can compensate for the injury-induced rapid loss of NMNAT2, the endogenous axonal NMNAT [28]. NMNAT2 in turn, inhibits SARM1, an inducible NAD^+ cleavage enzyme (NADase) that is the central executioner of axon degeneration [28-32]. Hence, mutations in NMNAT1 may promote retinal degeneration through the direct impact on NAD^+ biosynthesis and/or through the regulation of the SARM1-dependent degenerative program.

In this study, we determined the cell types and molecular mechanisms that cause retinal degeneration in LCA9. Using NMNAT1 conditional mutant mice, we showed that photoreceptors degenerate rapidly after the loss of NMNAT1 and that depletion of NMNAT1 in rod or cone cells, but not in RPE cells, is necessary and sufficient for the retinal degeneration. With the relevant cell type identified, we tested the therapeutic potential of AAV-mediated gene replacement, an FDA-approved approach for LCA2 and an area of intense interest in the retinal degeneration field [33-36]. Using a variant of AAV8 [37,38], we found that gene replacement of NMNAT1 in photoreceptors ameliorates the retinal degeneration and visual impairment caused by loss of NMNAT1. Finally, we determined the mechanism by which loss of NMNAT1 leads to photoreceptor degeneration. Loss of NMNAT1 leads to activation of SARM1 in photoreceptors, much as loss of NMNAT2 leads to SARM1 activation in axons [39]. Moreover,

photoreceptor degeneration is mediated by SARM1 in the absence of NMNAT1, much as axon degeneration and perinatal lethality is mediated by SARM1 in the absence of NMNAT2 [28,31]. Hence, photoreceptor neurodegeneration in LCA9 shares a deep mechanistic similarity to the pathological axon degeneration pathway. Since the SARM1 pathway is likely druggable [40,41], these findings provide a framework for developing new therapeutic strategies for treating patients with LCA9 and potentially other retinal disorders.

Results

NMNAT1 is a nuclear enzyme that synthesizes NAD^+, an essential metabolite that is central to all aspects of cellular metabolism. NMNAT1 is indispensable for mouse development [42] and recent studies identified causative mutations in *NMNAT1* in patients with Leber congenital amaurosis type 9 (LCA9), a disorder associated with severe, early-onset retinal degeneration and vision loss [1-6]. Patients with LCA9 have no systemic involvement outside the eye, suggesting that population(s) of cells within the retina are particularly vulnerable to the loss of NMNAT1 function. To investigate the role of NMNAT1 in retinal homeostasis, we first determined its expression pattern in the retina using mutant mice expressing an NMNAT1-lacZ fusion protein without the nuclear localization signal. Mice heterozygous for this mutant allele were viable and were used to map NMNAT1 expression by staining retinal sections with X-gal. LacZ staining was detected in the retinal pigment epithelium (RPE), photoreceptor outer segments (OS), inner segments (IS), outer nuclear layer (ONL), outer plexiform layer (OPL), inner nuclear layer (INL), inner plexiform layer (IPL), and ganglion cell layer (GCL) suggesting the ubiquitous expression of NMNAT1 in retina (Figure 1A).

To investigate the effects of NMNAT1 deletion on the retina, we generated *Nmnat1*$^{fl/fl}$*:ActCre*^{ERT2} mice by breeding mice harboring an *Nmnat1* floxed allele (*Nmnat1*^{fl}) with the *ActCre*^{ERT2} mice that express Cre recombinase globally via the actin promoter that is activated by tamoxifen. Since NMNAT1 deficient embryos do not survive [42], we treated 2-month-old *Nmnat1*$^{fl/fl}$*:ActCre*^{ERT2} and control mice with tamoxifen. We first used RT-PCR to measure *Nmnat1* mRNA in the retina at 21 days after tamoxifen and found that it was significantly decreased in NMNAT1 cKO (*Nmnat1*$^{fl/fl}$*:ActCre*^{ERT2} + tamoxifen) compared with wild type (WT) mice (Figure 1B). Then we measured NAD^+ metabolites in the retina at 4 weeks

after tamoxifen injection and found increases in NMN and nicotinamide (Nam), the precursors of NAD^+, and a slight decrease in NAD^+ in NMNAT1 cKO mice. (Figure 1C, D, E). We next evaluated retinal pathology at 4 weeks after *Nmnat1* excision using biomicroscopy. Fundus images showed abnormalities including attenuation of blood vessels (Figure 2A, B arrowhead) and the appearance of a honeycomb structure, suggesting exposure of retinal pigment epithelium (RPE) cells (Figure 2A, B arrow) in the mutant animals. These vascular abnormalities were further examined using fluorescein angiography which demonstrated microvascular and macrovascular abnormalities associated with vascular leakage in NMNAT1 cKO eyes (Figure 2C, D arrowheads). Histopathological examination of the retina with hematoxylin and eosin (HE) stained sections showed severe retinal degeneration as evidenced by the cell loss in outer and inner nuclear layers (ONL and INL) at 4 weeks post tamoxifen treatment, suggesting the loss of photoreceptor cells and interneurons (Figure 2E, F). These results suggest that the photoreceptor cells and interneurons are highly vulnerable following the loss of NMNAT1.

To gain further insights into the temporal aspects of the retinal degenerative process, we analyzed retinal morphology at multiple time points after tamoxifen administration. The loss of nuclei in the ONL and INL layers were evident at 25 days post tamoxifen injection and robust retinal thinning was evident at 33 days post tamoxifen injection (Figure 3A). Next, we measured layer-specific cell losses over time by counting the number of cell nuclei. This analysis showed that cell loss in the ONL (photoreceptor cells) was much more severe than that observed in the INL (interneurons) (Figure 3B). Cell loss was first detected in the ONL around 3 weeks after tamoxifen administration and gradually increased such that only ~15% of the cells remained at 33 d. Nuclear counts in the INL also revealed cell losses but these were less severe (~35% remaining at 33 d) (Figure 3A, B). To examine the type of cell death occurring after NMNAT1 loss, we performed TUNEL staining. We found evidence of apoptosis in the ONL but not in the INL even at later stages, suggesting that an apoptotic mechanism is at least partially responsible for the loss of photoreceptor cells in NMNAT1-deficient retinas (Figure 3C).

Next, we evaluated retinal function after NMNAT1 deletion using electroretinogram

(ERG). We examined three cohorts of mice: *Nmnat1*$^{fl/fl}$*:ActCre*^{ERT2} treated with tamoxifen, untreated *Nmnat1*$^{fl/fl}$*:ActCre*^{ERT2} or *Nmnat1*$^{fl/fl}$ treated with tamoxifen. In mutant animals in which NMNAT1 was excised, we observed a complete loss of both scotopic (rod-driven responses) and photopic (cone-driven responses) responses, indicating the loss of Nmnat1 in mature retina causes severe photoreceptor dysfunction (Figure 3D-F). This is consistent with previous reports showing developmental retinal defects in the tissue specific NMNAT1 knockout mice [11,12]. While previous reports show that NMNAT1 is necessary for appropriate retinal development, our pathological and functional analyses of two-month-old mice show that NMNAT1 is necessary for photoreceptor cell maintenance and mature retinal functions.

In addition to NMNAT1, mammalian cells encode two other NMNAT isoforms; NMNAT2 that is localized in the Golgi and cytosol, and NMNAT3 that is localized inside the mitochondria. Since the loss of NMNAT1 induced retinal degeneration, we sought to determine the role of NMNAT2 and 3 in the retinal structure/function. A previous study showed that NMNAT2 knockout mice are perinatally lethal and have truncated optic nerves as well as peripheral axon degeneration [43]. We could not assess the role of NMNAT2 in retinal function due to the lack of conditional knockout mice. On the other hand, NMNAT3 deficient mice (Nmnat3^{KO}) are viable with splenomegaly and hemolytic anemia [44]. Mitochondrial dysfunction is associated with various retinal diseases including diabetic retinopathy, glaucoma and age-related macular degeneration [45,46]. We generated Nmnat3^{KO} mice and investigated their retinal function using ERG. Consistent with the previous report, NMNAT3^{KO} mice showed splenomegaly (data not shown), however, there were no defects in ERG (Supplemental Figure1). These results indicate that NMNAT3 is dispensable for retinal function, suggesting NMNAT1 is the functionally dominant isoform controlling retinal phenotype.

Identifying the cells that are vulnerable to NMNAT1 loss is key to understanding LCA9 pathogenesis. The high expression of NMNAT1 in photoreceptors (Figure 1C) and the severe loss of the ONL induced by NMNAT1 deletion prompted us to test whether loss of NMNAT1 specifically in photoreceptors would result in their death and recapitulate the phenotype observed using the widely expressed *ActCre*^{ERT2}. We therefore generated mice lacking NMNAT1 specifically in rod photoreceptors (NMNAT1 Rho-Cre) by crossing the *Nmnat1*$^{fl/fl}$

mice with Rhodopsin-iCre75 mice in which Cre recombinase expression is driven by the rhodopsin promoter starting postnatally at P7 [47]. We analyzed the retinas of *Nmnat1*$^{fl/fl}$:Rhodopsin-Cre mice at 6-weeks-of-age. Similar to previous findings [11,12], histological analysis revealed severe thinning of the ONL in these mutant mice (Figure 4A, B), with a significant reduction in cell number as detected by nuclear counts (Figure 4E). There was also a much smaller decrease in the number of cells in the INL. Consistent with the loss of ONL cells, ERG analysis showed a severe reduction in the scotopic-a and –b waves, representing rod photoreceptor function, in the *Nmnat1*$^{fl/fl}$:RhodopsinCre mice. In addition, we found decreases in cone mediated photoresponses (photopic b-wave signal) (Figure 4F-H), that is likely secondary to a loss of cone photoreceptor cells due to loss of required rod-derived survival factors [9,48].

To further explore the importance of NMNAT1 activity in cones, we deleted NMNAT1 in these cells using cone-specific Cre mice. We crossed *Nmnat1*$^{fl/fl}$ mice with HGRP-Cre mice in which Cre recombinase expression is driven by the human red/green pigment promoter starting at P10 [49]. At 6-weeks-of-age we examined these mutant mice histologically, but did not detect any gross abnormalities, presumably due to the low number of cones (only 3% of total photoreceptors) in mice (Figure 4C, D, I). However, ERG analysis showed a complete loss of the photopic-b wave, which is derived from cone photoreceptors. This functional result clearly shows that NMNAT1 activity is vital for cone function (Figure 4J-L). In summary, these genetic ablation experiments demonstrate the importance of NMNAT1 for proper function of both rods and cones, and indicate that LCA9-associated retinal degeneration is likely due to the direct cell-autonomous effects of *NMNAT1* mutations in photoreceptors.

Photoreceptors are dependent on RPE cells to regenerate the chromophore 11-cis-retinal from all-trans-retinal via the visual cycle that is essential for the regeneration of light-sensing rhodopsin. Mutations in RDH5, which is located in the RPE cells and is a key enzyme in the visual cycle, lead to the cone and rod dysfunction [50]. RDH5 is an NAD^+ dependent enzyme, suggesting that NMNAT1 loss in RPE cells could impact retinal function by influencing activity of this key enzyme. RPE cells also contribute to photoreceptor outer segment nourishment, and the interruption of this process is another potential cause of retinal

degeneration [51]. To investigate whether the loss of NMNAT1 in RPE cells could also contribute to retinal degeneration, we depleted NMNAT1 specifically from these cells. We crossed *Nmnat1*$^{fl/fl}$ mice with Vmd2-Cre mice (kindly provided by Dr. Thomas Ferguson at Washington University, St. Louis, MO) in which Cre recombinase is specifically expressed in RPE cells [52] to produce *Nmnat1*$^{fl/fl}$*:Vmd2Cre* mice. We examined 16-week-old mutant mice and found no histological abnormalities in the retina. Cell counts in both the ONL and INL were normal. Both the scotopic and photopic responses were indistinguishable from wildtype mice (Figure 5A-E). These results indicate that NMNAT1 loss in RPE cells does not contribute to photoreceptor loss and retinal degeneration seen in LCA9.

Loss of function studies indicated crucial roles for NMNAT1 in photoreceptor survival and retinal function. To further explore these findings and examine the utility of gene replacement therapy in LCA9, we subretinally delivered AAV8(Y733F) containing the photoreceptor specific human rhodopsin kinase (hGRK1) promoter driving HA-tagged human NMNAT1 [37,38]. An analogous vector expressing GFP was used as a control. Virus was injected into the subretinal space of two-month-old wildtype mice. Transgene expression was evaluated 4-6 weeks post-injection. AAV-mediated GFP expression was observed in a subset of rhodopsin-positive cells but was weak in the inner nuclear layer (INL) (Supplemental Figure 2A). These results confirm earlier reports that the hGRK1 promoter restricts transgene expression to photoreceptors. We next asked whether AAV-NMNAT1 could prevent the retinal degeneration caused by NMNAT1 excision. Two-month-old Nmnat1$^{fl/fl}$*;ActCre*^{ERT2} *mice* received subretinal injections of AAV-NMNAT1 in one eye, and control vector (AAV-GFP) in the contralateral eye. We confirmed the expression of NMNAT1-HA in a subset of outer nuclear cells and minor population of inner nuclear cells using HA epitope tag antibody (Supplemental Figure 2B, C). Mice that received AAV-NMNAT or AAV-GFP were then treated with tamoxifen to deplete endogenous NMNAT1. One month after tamoxifen treatment, we examined retinal function and performed histological analysis. Retinas injected with AAV-GFP showed severe thinning of retinal layers, particularly the ONL, analogous to that observed in tamoxifen treated mutant animals without viral injection (Figure 6A and Figure 2F). However, in eyes injected with AAV-NMNAT1, the retinal layers were better preserved (Figure 6A). Quantification of nuclei in the ONL showed significant increase of photoreceptor survival in

AAV-NMNAT1 treated eyes relative to controls; however, we observed no significant difference in nuclear numbers within the INLs of these animals (Figure 6B). Finally, we tested whether treatment with AAV-NMNAT1 provided functional recovery. ERGs were performed on mutant animals treated with tamoxifen and injected subretinally with either AAV-NMNAT1 or AAV-GFP. Despite only a subset of the retina being transduced by subretinally delivered AAV-NMNAT1, we observed significantly increased scotopic a-wave amplitudes in AAV-NMNAT1 treated retinas compared with retinas injected with AAV-GFP (Figure 6C) accompanied by a small increase in the scotopic and photopic b-wave amplitudes between AAV-NMNAT1 and AAV-GFP treated retinas (Figure 6D, E). In summary, NMNAT1 gene delivery to photoreceptor cells significantly improved their survival and function in this LCA9 model, potentially providing an exciting new avenue for therapy.

We next sought to determine the molecular mechanisms required for retinal degeneration in the NMNAT1-deficient retina. The loss of NMNAT2 induces an increase in NMN that is hypothesized to activate SARM1-dependent axon degeneration [53,54]. Our metabolomic analysis revealed that NMN is increased in the NMNAT1-deficient retinas (Figure 1D), and previous studies have detected SARM1 in mouse and bovine photoreceptor cells [55-57]. These results raise the possibility that the increased retinal NMN activates SARM1 and induces NAD^+ loss and cellular degeneration in the retina. To test this hypothesis, we crossed *Nmnat1*$^{fl/fl}$*:ActCre*^{ERT2} mice with SARM1 knockout mice [58] to generate *Nmnat1*$^{fl/fl}$*:ActCre*^{ERT2}*:Sarm1*^{KO} mice. NMNAT1 was excised in these mice via tamoxifen administration at 2 months of age (NMNAT1 cKO: SARM1 KO). Consistent with previous results (Figures 2, 3), the number of ONL nuclei was reduced at 32 d post tamoxifen injection in NMNAT1 cKO retina (Figure 7A). In sharp contrast, there was no loss of ONL cells in NMNAT1 cKO: SARM1 KO retina (Figure 7A, B). We next examined the functional consequences of NMNAT1 depletion in the presence or absence of SARM1 using ERGs, and again found that loss of SARM1 prevented the severe loss of both scotopic and photopic responses due to NMNAT1-deficiency (Figure 7C-E). These results indicate that SARM1 is crucial for the retinal degeneration due to NMNAT1-deficiency.

We recently reported that cADPR is a biomarker of SARM1 activity [39]. After neuronal

injury, SARM1 is activated and intracellular cADPR is increased in a SARM1 dependent manner [39]. We observed a significant increase in cADPR in NMNAT1 cKO and this increase was completely blocked in the NMNAT1 cKO:SARM1 KO retina (Figure 7H). Concomitant with this rise in cADPR and further evidence of increased SARM1 NADase activity after loss of NMNAT1, we observed reductions in NAD^+ in NMNAT1 cKO and NMNAT1 cKO:SARM1 KO mice (Figure 7F). We also observed increases in NMN, which is postulated to induce activation of SARM1. This increase is consistent with the loss of NMNAT1, which normally converts NMN to NAD^+ (Figure 7G). The increase of NMN was larger in NMNAT1 cKO: SARM1KO compared with NMNAT1 cKO likely because NMNAT1-deficient cells were lost in NMNAT1 cKO but not in NMNAT1 cKO: SARM1 KO retina. Hence, loss of NMNAT1 leads to the activation of SARM1, and SARM1 is required for the subsequent photoreceptor degeneration. Therefore, the essential function of NMNAT1 in photoreceptors is to inhibit SARM1, and inhibition of SARM1 is a candidate therapeutic strategy for the treatment of LCA9.

Discussion

In this study, we demonstrate that deletion of NMNAT1 in the adult retina causes a dramatic loss of photoreceptors and a concomitant reduction in retinal function. In addition, cell-type specific deletion of NMNAT1 in early postnatal photoreceptors is sufficient to induce retinal degeneration. Hence, NMNAT1 is required for the survival and function of both developing and mature photoreceptors. Using a modified AAV8 vector and the human rhodopsin kinase promoter to express NMNAT1, we demonstrated that a gene replacement strategy can improve retinal structure and function in this model of LCA9. Finally, we defined the molecular mechanism by which NMNAT1 promotes photoreceptor function and survival. In photoreceptors, loss of NMNAT1 leads to activation of the inducible NADase SARM1 and the SARM1-dependent degeneration of photoreceptors. This finding defines a common mechanism for photoreceptor degeneration and pathological axon degeneration. Loss of NMNAT1 in photoreceptors or NMNAT2 in axons leads to the SARM1-induced death of photoreceptors or axons, respectively. This surprising result extends our understanding of both the mechanisms causing retinal degeneration and the potential role of SARM1 in human disease [59].

Retinal NAD^+ homeostasis is crucial for visual function and NAD^+ decline is a hallmark of many retinal degenerative disease models [9]. Reduced NAD^+ induces mitochondrial dysfunction in photoreceptor cells and affects activity of SIRT3, which protects the retina from light-induced and other forms of neurodegeneration. In addition, NAD^+-dependent enzymes play crucial roles in phototransduction including the regeneration of the photosensitive element, 11-cis-retinal, and the regulation of photoreceptor membrane potential. Moreover, mutations in the genes encoding some of these enzymes cause retinal degenerative disease. For example, mutations in all-trans-retinal dehydrogenase (RDH12) that is localized to photoreceptor cells are associated with LCA13. Combined deletion of retinal dehydrogenases, RDH12 and RDH8, results in mouse retinal degeneration [60]. NAD^+ is also a cofactor for inosine monophosphate dehydrogenase (IMPDH1), which is the rate limiting enzyme for GTP synthesis and, in turn, is required for cGMP production. cGMP is indispensable for the regulation of photoreceptor membrane potential and calcium concentration upon light stimulation. IMPDH1 mutations cause both a dominant form of retinitis pigmentosa (RP10) and LCA11. These results highlight the central role of NAD^+ metabolism in the photoreceptor.

NMNAT1 is the only NMNAT enzyme localized to the nucleus in mammals and is crucial for nuclear NAD^+ synthesis. Despite the broad functions of nuclear NAD^+ in all cell types, the sole consequence of LCA9-associated *NMNAT1* mutations is retinal dysfunction/degeneration without systemic abnormalities. Previous studies, and our results, show early loss of photoreceptor cells in NMNAT1-deficient retina [11,12]. In photoreceptors NMNAT1 localizes not only in the nucleus but also near the basal body of the cilia [11], suggesting a unique role of extra-nuclear NMNAT1 in the photoreceptor cells that may explain photoreceptor specific pathology in LCA9 patients. Consistent with this hypothesis, a subcellular proteomics study showed the existence and enrichment of NMNAT1 in the photoreceptor outer segments [56]. Single-cell transcriptomic RNA analysis also found *Nmnat1* in rods and cones [57,61]. Consistent with an extranuclear role for NMNAT1 in photoreceptors in these studies, cytosolic NMNAT2 was either not identified or was found at much lower levels than NMNAT1. NMNAT3 is the mitochondrial NMNAT, and we show here that it is dispensable for retinal homeostasis and function, further highlighting the central requirement for NMNAT1 in photoreceptors.

Having demonstrated that NMNAT1 is required in photoreceptors in this model of LCA9, we tested the efficacy of viral mediated gene replacement as a candidate therapeutic. Adeno associated virus (AAV) is a naturally occurring, non-pathogenic virus used in gene therapy studies to restore structure and function to diseased cells. Recently, the U.S. FDA approved an AAV-RPE65 vector as a therapeutic reagent for LCA2 and other biallelic RPE65 mutation associated retinal dystrophies [35]. Theoretically, LCA9 caused by the loss of NMNAT1 function is a reasonable target for AAV mediated gene therapy. To achieve expression in photoreceptors, we used an AAV8 variant that is a highly efficient for transducing photoreceptors following subretinal injection as well as the hGRK1 promoter that has activity exclusively in rods and cones [37,38]. Delivery of AAV8(Y733F)-hGRK1-NMNAT1 significantly improved the retinal phenotype of mice deficient for NMNAT1. Although the functional recovery was partial, these results are quite encouraging since this mouse model involves complete deletion of NMNAT1, while many LCA9 patients have compound heterozygous mutations that are expected to retain partial function [7].

Since NAD^+ plays such a central role in photoreceptors, the identification of the NAD^+ biosynthetic enzyme NMNAT1 as the cause of LCA9 suggests that photoreceptor degeneration in LCA9 is due the reduction in NAD^+ synthesis. Surprisingly, we demonstrate here that this is not the essential function for NMNAT1 in photoreceptors. Instead, NMNAT1 is required to restrain the activity of the prodegenerative NADase SARM1. When NMNAT1 is deleted from SARM1 KO photoreceptors, the photoreceptors do not die and maintain their physiological function, demonstrating that these cells do not require NMNAT1 as long as SARM1 is not present. This finding is perfectly analogous to the relationship between NMNAT2 and SARM1 in the axon. NMNAT2 KO mice are perinatal lethal and have dramatic axonal defects, but NMNAT2, SARM1 double KO mice are viable and have a normal lifespan [31]. NMNAT enzymes inhibit the activation of SARM1 [30], potentially by consuming the NAD^+ precursor NMN, which is postulated to activate SARM1 [53,54]. Prior to our study, loss of NMNAT2 was the only known trigger of SARM1 activation. Our current work suggests that SARM1 is activated by the loss of any NMNAT enzyme whose activity is not redundant with another NMNAT isoform. NMNAT2 is the only cytosolic NMNAT in the axon, and so loss of

axonal NMNAT2 leads to localized activation of SARM1 and axon degeneration. In photoreceptors, NMNAT1 is not only nuclear but also extranuclear, and NMNAT2 is apparently present at very low levels. Hence, in photoreceptors loss of NMNAT1 triggers activation of SARM1 which consumes NAD^+ and triggers cell death. As NAD^+ loss is a common pathology of many retinal diseases, this raises the possibility that SARM1 activation may contribute to a wide range of retinal disorders. In support of this conjecture, recent studies found that SARM1 promotes retinal degeneration in X-linked retinoschisis [62] and rhodopsin-deficient mice [63].

Our identification of SARM1 as the executioner of photoreceptor death in this model of LCA9 opens up new therapeutic possibilities. We previously developed a potent dominant negative SARM1 variant and demonstrated that AAV-mediated expression of dominant negative SARM1 strongly protects injured axons from degeneration in the peripheral nervous system [64] and is also effective in a neuroinflammatory model of glaucoma [65]. While NMNAT1 gene replacement is an exciting treatment option for LCA9, if SARM1 plays a more general role in retinal degeneration, then using gene therapy to express this dominant negative SARM1 could not only treat LCA9, but also multiple retinal neurodegenerative diseases. In addition, SARM1 is an enzyme and so small molecule enzyme inhibitors would be another attractive treatment modality [40,41]. These findings demonstrate the utility of dissecting the molecular mechanism of degeneration in diseases of retinal neurodegeneration. In the case of LCA9, these studies identified a SARM1-dependent photoreceptor cell death pathway and discovered the heretofore unknown commonality between the mechanism of retinal neurodegeneration and pathological axon degeneration.

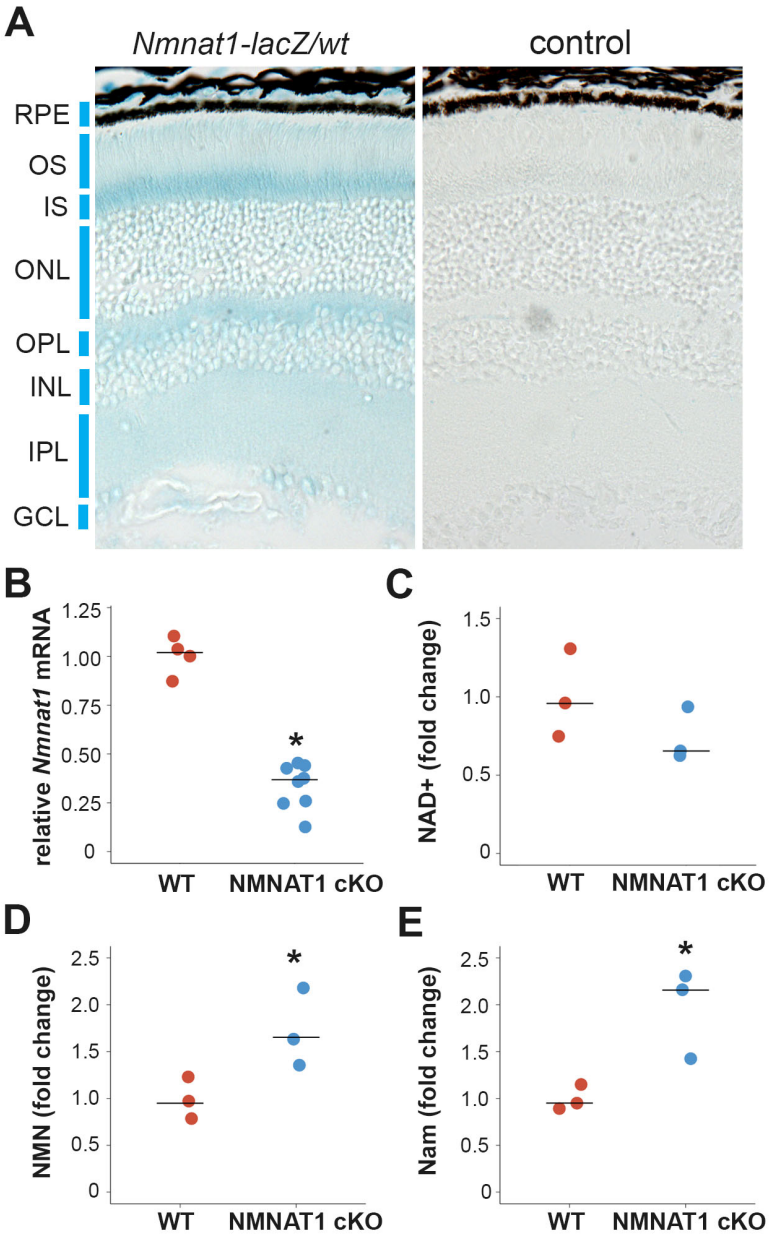

Figure 1. NMNAT1 **is ubiquitously expressed in the retina and its depletion induced alterations in NAD⁺ metabolites.** (A) X-Gal staining of retinal tissues from mice heterozygous for Nmnat-lacZ fusion protein lacking the nuclear localization signal (*Nmnat1-lacZ/wt*) or wild type mice (control). (B) Quantitative RT-PCR analysis of *Nmnat1* mRNA in retinal tissues from wild type (WT) or *Nmnat1*$^{fl/fl}$*: ActCre*^{ERT2} mice at 21 days post tamoxifen injection (NMNAT1 cKO) showed significant reduction of *Nmnat1* mRNA compared with WT. * $p<0.05$ denotes the significant difference from WT with Mann-Whitney U test (n = 8 for NMNAT1 cKO (4 mice) and n = 4 for WT (2 mice), two technical replicates for each mouse). (C, D, E) Metabolite analysis by LC-MSMS in retinal tissues from wild type (WT) or NMNAT1 cKO mice 25 days post tamoxifen injection in *Nmnat1*$^{fl/fl}$*: ActCre*^{ERT2}. Fold changes of NAD^+ (C), NMN (D), and nicotinamide (Nam) (E) concentration compared with that of WT retinal tissues are shown.

*$p<0.05$ denotes the significant difference from WT with Kruskal-Wallis test ($n = 3$ for NMNAT1 cKO or WT). Graphs show the all data points and median (cross bars).

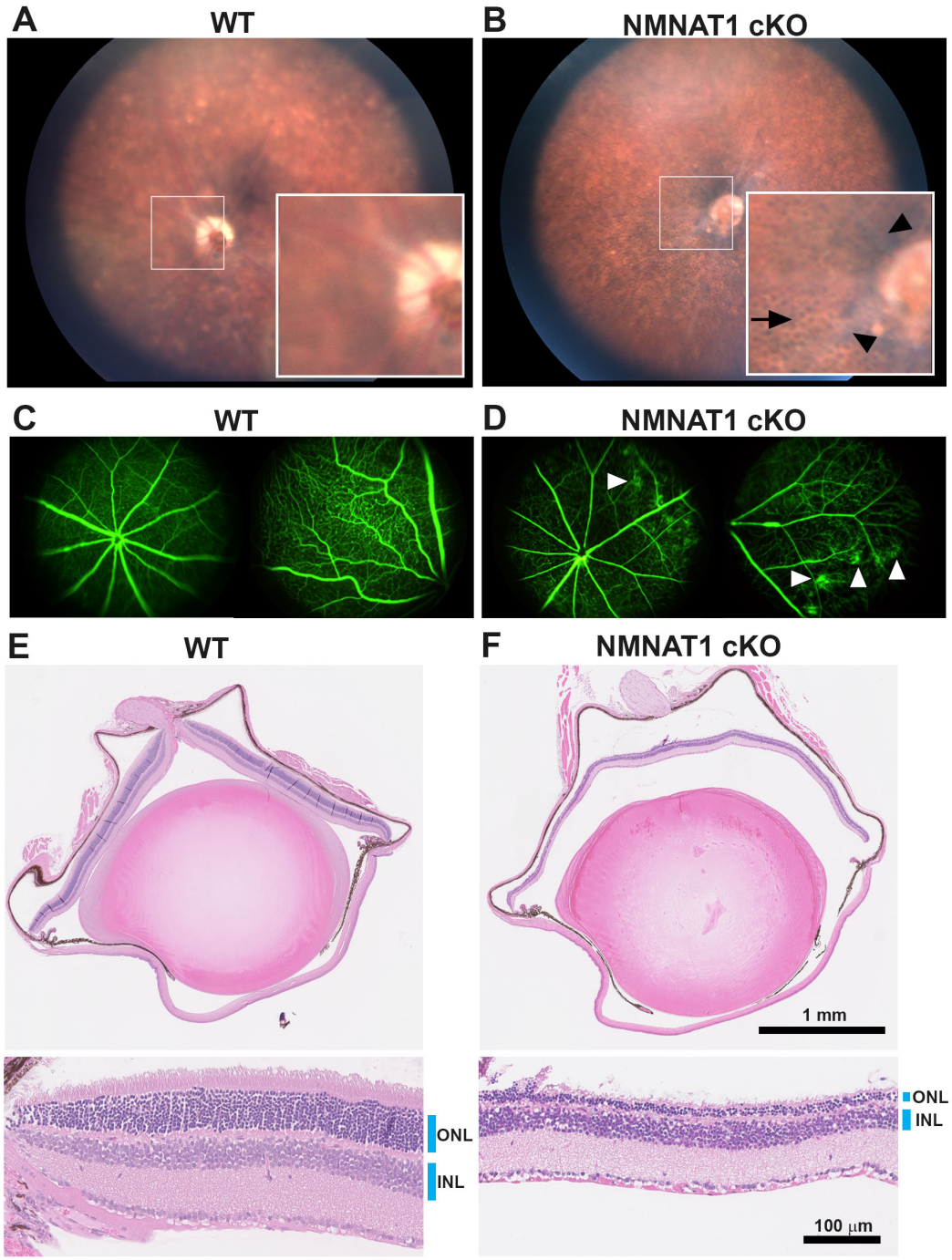

Figure 2. NMNAT1 depletion induces severe retinal degeneration. (A, B) Fundus biomicroscopy images of the retina from wild type (WT, A) or NMNAT1 knock out (NMNAT1 cKO, B) mice at 4 weeks post tamoxifen injection. (C, D) Fluorescent angiogram images of the retina from wild type (WT, C) or NMNAT1 knock out (NMNAT1 cKO, D) mice at 4 weeks post tamoxifen injection. Arrowheads indicate vascular leakage and arrows indicate the honeycomb structures. (E, F) hematoxylin and eosin stained eye sections from wild type (WT, E) or NMNAT1 knock out (NMNAT1 cKO, F) mice at 4 weeks post tamoxifen injection. Outer nuclear layer (ONL) and inner nuclear layer (INL). Note the substantial thinning of the ONL.

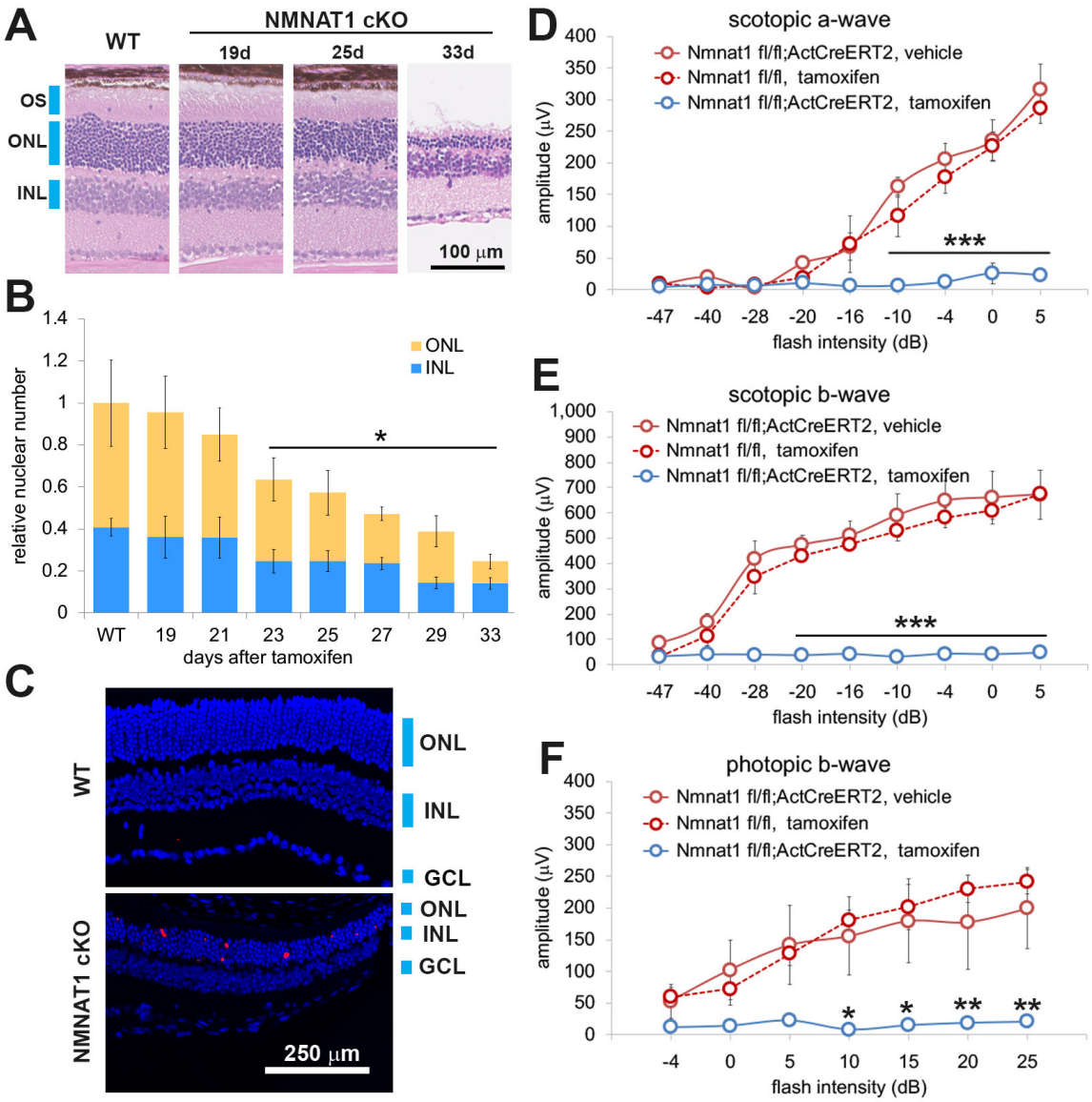

Figure 3. NMNAT1 induces the loss of photoreceptor cells and retinal function. (A) Representative images of hematoxylin/eosin stained sections showing time course of retinal degeneration in NMNAT1 cKO mice at 19 to 33 days post tamoxifen injection or littermate control mice at 33 days post tamoxifen injection (WT). Blue bars indicate outer nuclear layer (ONL), inner nuclear layer (INL), and outer segment. (B) Quantification of relative outer nuclear layer (ONL) and inner nuclear layer (INL) nuclei numbers compared with WT at various time after tamoxifen injection. Graphs show the average and error bars represent the standard deviation. Statistical analysis was performed by one-way ANOVA with Holm-Bonferroni multiple comparison (n=3 for WT, 19d, 21d, and n=4 for 25d, 27d, and n=2 for 33d INL, and n=3 for 33d ONL). $F(7, 70) = 20$, $p=2.2\times10^{-14}$ for ONL and $F(7,67) = 23$, $p=2.2\times10^{-15}$ for INL. * $p<0.05$ denotes the significant difference compared wild type (WT). (C) Representative images of TUNEL staining in WT (*Nmnat1*$^{fl/fl}$*: ActCre*^{ERT2} without tamoxifen) or NMNAT1 cKO mice (*Nmnat1*$^{fl/fl}$*: ActCre*^{ERT2} 29 days post tamoxifen injection). Blue bars indicate outer nuclear layer

(ONL), inner nuclear layer (INL), and ganglion cell layer (GCL). (D, E, F) ERG analysis of controls (*Nmnat1*$^{fl/fl}$*:ActCre*^{ERT2} vehicle or *Nmnat1*$^{fl/fl}$ tamoxifen) and SARM1 cKO (*Nmnat1*$^{fl/fl}$*:ActCre*^{ERT2} tamoxifen). Graphs show the average and error bars represent the standard error. Scotopic a-wave (D), scotopic b-wave (E), and photopic b-wave (F) are shown. Statistical analysis was performed by two-way ANOVA with Tukey post-hoc test (n = 3 for *Nmnat1*$^{fl/fl}$*:ActCre*^{ERT2} with vehicle and n = 3 for *Nmnat1*$^{fl/fl}$ 33 days post tamoxifen injection and n = 4 for *Nmnat1*$^{fl/fl}$*:ActCre*^{ERT2} 33 days post tamoxifen injection). $F(8, 72) = 27$, $p < 2x10^{-16}$ between controls and NMNAT1 cKO for scotopic a wave, $F(8, 72) = 61$, $p<2.7x10^{-15}$ between controls and NMNAT1 cKO for scotopic b wave, $F(6, 56) = 10$, $p = 0.026$ between controls and NMNAT1 cKO for photopic b wave. * $p <0.05$, ** $p < 0.001$, and *** $p < 0.0001$ denote a significant difference compared with WT.

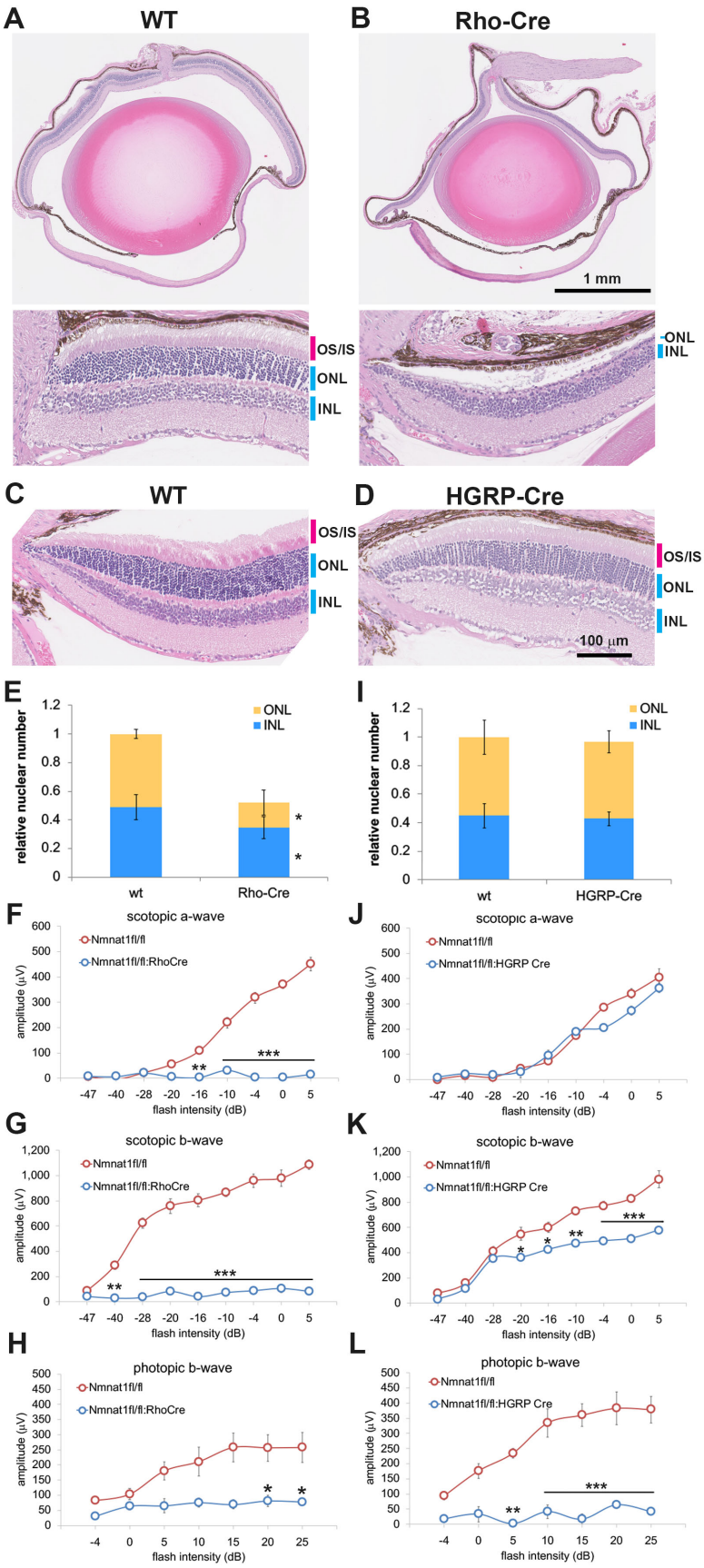
A
WT
B
Rho-Cre
1 mm
OS/IS
ONL
INL
C
WT
D
HGRP-Cre
100 μm
E
relative nuclear number
wt
Rho-Cre
I
HGRP-Cre
F
scotopic a-wave
Nmnat1fl/fl
Nmnat1fl/fl:RhoCre
amplitude (μV)
flash intensity (dB)
J
Nmnat1fl/fl:HGRP Cre
G
scotopic b-wave
K
H
photopic b-wave
L

Figure 4. Photoreceptor specific depletion of NMNAT1 induces retinal degeneration. (A, B, C, D) Hematoxylin and eosin stained eye sections from 6 week old wild type (WT, A, C), *Nmnat1$^{fl/fl}$:Rho-Cre* (rod-specific, Rho-Cre, B), or *Nmnat1$^{fl/fl}$:HGRP-Cre* (cone-specific, HGRP-Cre, D) mice. Blue bars indicate outer nuclear layer (ONL) and inner nuclear layer (INL). Red bars indicate the outer segments (OS) and inner segments (IS). (E) Quantification of relative ONL and INL nuclei numbers in WT or *Nmnat1$^{fl/fl}$:Rho-Cre* (Rho-Cre) retinas. Graphs show the average and error bars represent the standard deviation. *P<0.05 denotes the significant difference of the Rho-Cre retina compared with WT by Mann-Whitney U test (n = 2 for WT and n = 3 for Rho-Cre). (F, G, H) ERG analysis of WT or *Nmnat1$^{fl/fl}$:Rho-Cre* (Rho-Cre) mice. Scotopic a-wave (F), scotopic b-wave (G), and photopic b-wave (H) are shown. Graphs show the average and error bars represent the standard error. Statistical analysis was performed by two-way ANOVA with Tukey post-hoc test (n = 3 for WT or Rho-Cre). $F(8, 36) = 81$, $p < 2.0 \times 10^{-16}$ between WT and Rho-Cre for scotopic a wave, $F(8, 36) = 39$, $p < 1.9 \times 10^{-15}$ between WT and Rho-Cre for scotopic b wave, $F(8, 36) = 2.2$, $p = 7.2 \times 10^{-2}$ between WT and Rho-Cre for photopic b wave. * $p < 0.05$, ** $p < 0.001$, and *** $p < 0.0001$ denote a significant difference compared with WT. (I) Quantification of relative ONL and INL nuclei numbers in WT or *Nmnat1$^{fl/fl}$:HGRP-Cre* (HGRP-Cre) retinas. Graphs show the average and error bars represent the standard deviation. There is no significant difference between HGRP-Cre retinas compared to WT as assessed by Mann-Whitney U test (n = 4 for WT or HGRP-Cre). (J, K, L) ERG analysis of WT or *Nmnat1$^{fl/fl}$:HGRP-Cre* (Rho-Cre) mice. Scotopic a-wave (J), scotopic b-wave (K), and photopic b-wave (L) are shown. Graphs show the average and error bars represent the standard error. Statistical analysis was performed by two-way ANOVA with Tukey post-hoc test (n = 3 for WT or HGRP-Cre). $F(8, 36) = 3.5$, $p < 4.1 \times 10^{-3}$ between WT and Rho-Cre for scotopic a wave, $F(8, 36) = 7.7$, $p < 6.1 \times 10^{-6}$ between WT and Rho-Cre for scotopic b wave, $F(6, 28) = 6.9$, $p = 1.3 \times 10^{-4}$ between WT and Rho-Cre for photopic b wave. * $p < 0.05$, ** $p < 0.001$, and *** $p < 0.0001$ denote a significant difference compared with WT.

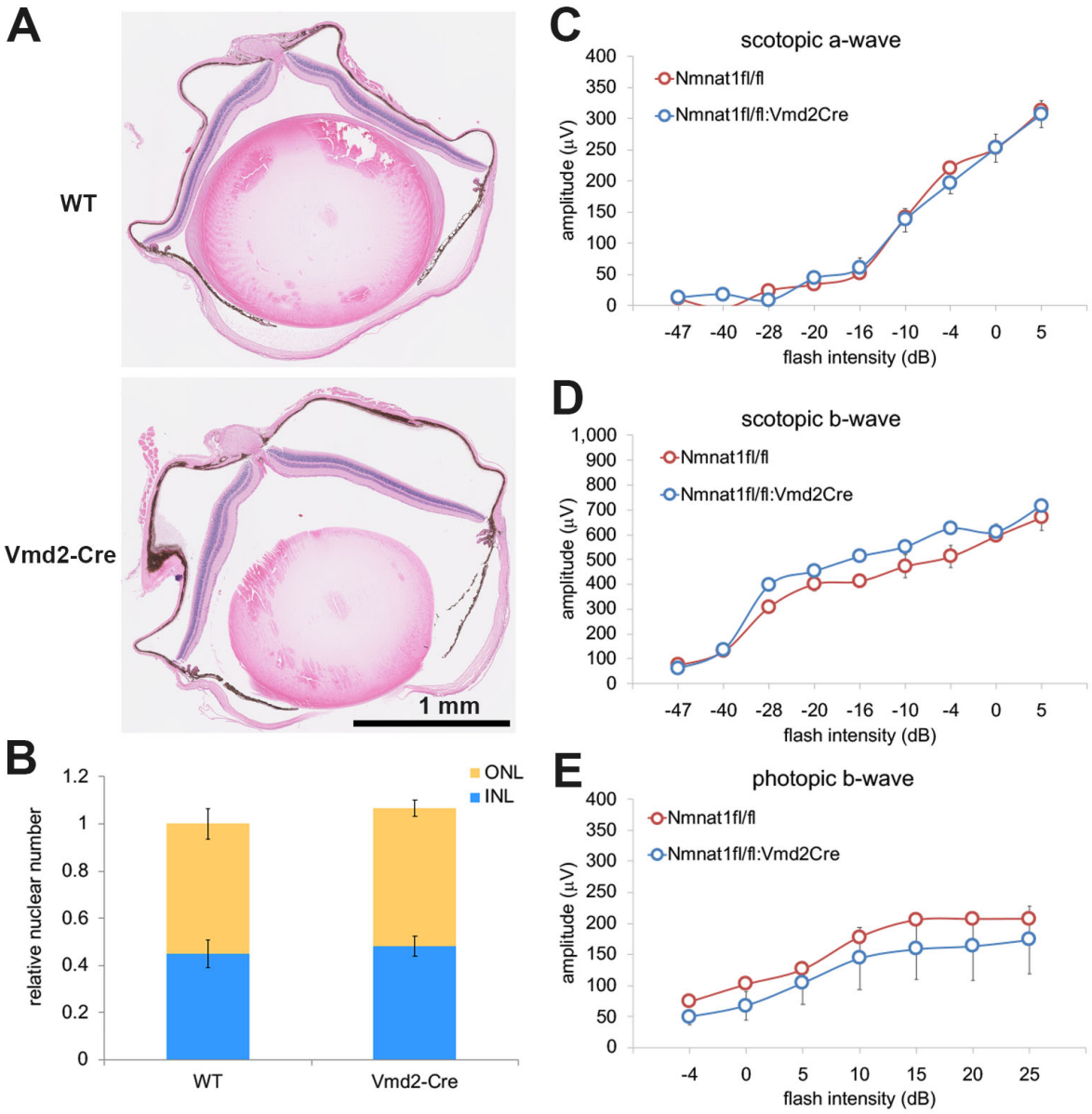

Figure 5. RPE specific deletion of NMNAT1 does not affect retinal morphology and function. (A) Hematoxylin and eosin stained eye sections from 16 weeks old wild type (WT) or *Nmnat1$^{fl/fl}$: Vmd2-Cre* (retinal pigment epithelium-specific, Vmd2-Cre) mice. (B) Quantification of relative outer nuclear layer (ONL) and inner nuclear layer (INL) nuclei numbers in WT vs Vmd2-Cre retina. Graphs show the average and error bars represent the standard deviation. There is no statistical difference between WT and Vmd2-Cre mice as assessed by Mann-Whitney U test (n = 3 for WT or Vmd2-Cre). (C, D, E) ERG analysis of WT and Vmd2-Cre mice. Scotopic a-wave (C), scotopic b-wave (D), and photopic b-wave (E) are shown. Graphs show the average and error bars represent the standard error. Statistical analysis was performed by two-way ANOVA with Tukey post-hoc test (n = 2 for WT and n = 4 for Vmd2-Cre). $F(8, 36) = 0.31$, $p < 0.96$ between WT and Vmd2-Cre for scotopic a wave, $F(8, 36) = 0.61$, $p = 0.76$ between WT and Vmd2-Cre for scotopic b wave, $F(6, 28) = 0.015$, $p = 1$

between WT and Vmd2-Cre for photopic b wave. There is no statistically significant difference between control and Vmd2-Cre mice.

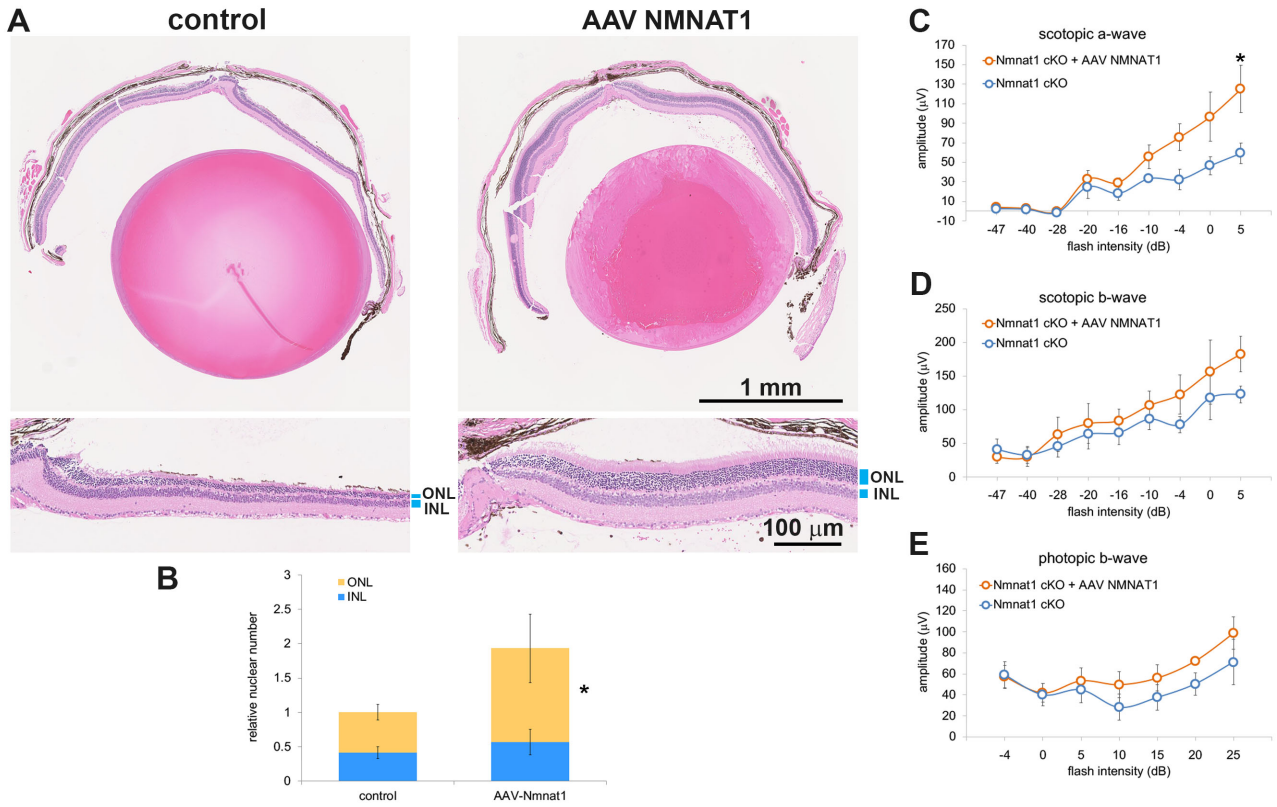

Figure 6. AAV-NMNAT1 partially rescued the retinal degeneration in NMNAT1-deficient retinas. (A) Hematoxylin and eosin stained eye sections from AAV-GFP (control) or AAV-NMNAT1 (AAV-NMNAT1) injected NMNAT1 cKO mice at 29 to 33 days post tamoxifen injection. Blue bars represent outer nuclear layer (ONL) and inner nuclear layer (INL). (B) Quantification of relative outer nuclear layer (ONL) and inner nuclear layer (INL) nuclei numbers of AAV-GFP (control) or AAV NMNAT1 (AAV-NMNAT1) administrated NMNAT1 cKO retina. Graphs show the average and error bars represent the standard deviation. *$p<0.05$ denotes the significant difference between the number of nuclei in ONL of AAV-NMNAT1 treated retinas vs controls by Mann-Whitney U test (n = 3 for control or AAV-NMNAT1). (C, D, E) ERG analysis of AAV-GFP (control) or AAV NMNAT1 (AAV- NMNAT1) administrated NMNAT1 cKO mice. Scotopic a-wave (C), scotopic b-wave (D), and photopic b-wave amplitudes (E) are shown. Graphs show the average and error bars represent the standard error. Statistical analysis was performed by two-way ANOVA with Tukey post-hoc test (n = 5 for control or AAV- NMNAT1). $F(8, 72) = 2.4$, $p = 0.022$ between control and AAV-NMNAT1 for scotopic a- wave, $F(8, 72) = 0.48$, $p = 0.86$ between control and AAV-NMNAT1 for scotopic b-wave, $F(6, 56) = 0.39$, $p = 0.88$ between controls and AAV-NMNAT1 for photopic b- wave. *$P<0.05$ denotes the statistical difference between WT and AAV-NMNAT1 mice.

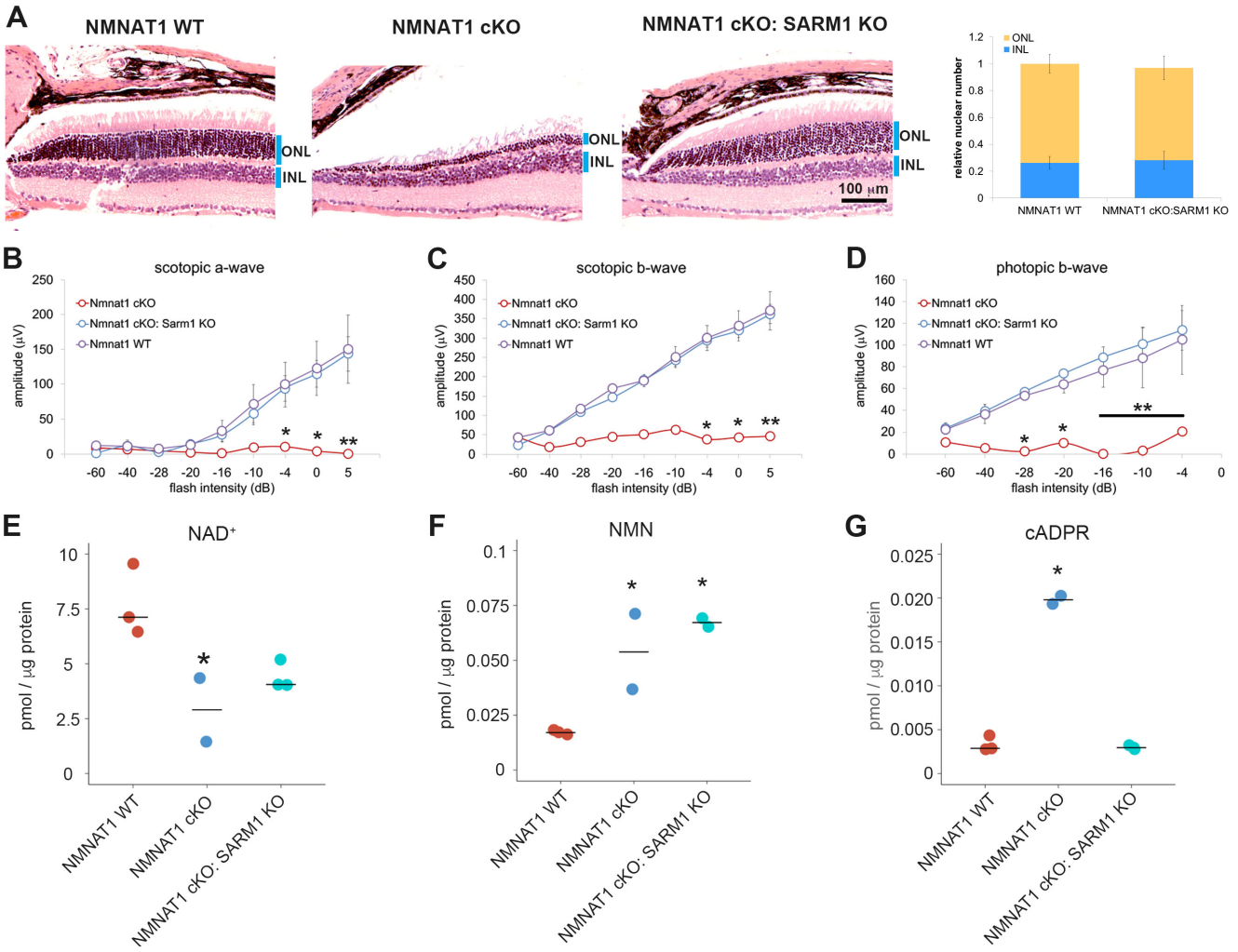

Figure 7. Depletion of SARM1 rescues retinal degeneration in the NMNAT1-deficient retina. (A) Hematoxylin and eosin stained eye sections from NMNAT1 WT (*Nmnat1$^{fl/fl}$: Sarm1$^{+/-}$*), NMNAT1 cKO (*Nmnat1$^{fl/fl}$: ActCre^{ERT2}* post 32 days tamoxifen injection), NMNAT1 cKO: SARM1 KO (*Nmnat1$^{fl/fl}$: SARM1$^{-/-}$: ActCre^{ERT2}* post 32 days tamoxifen injection). Blue bars represent outer nuclear layer (ONL) and inner nuclear layer (INL). (B) Quantification of nuclei numbers of inner (INL) and outer (ONL) nuclear layers. The graph shows the average and error bars of relative ONL and INL nuclei numbers of NMNAT1 WT or NMNAT1 cKO: SARM1 KO retina. No significant difference between NMNAT1 WT and NMNAT1 cKO: SARM1 KO by Mann-Whitney U test (n = 3 for each genotype). (C, D, E) ERG analysis of NMNAT1 WT (*Nmnat1$^{fl/fl}$: Sarm1$^{+/-}$* or *Nmnat1$^{fl/fl}$: Sarm1$^{-/-}$*), NMNAT1 cKO (*Nmnat1$^{fl/fl}$: ActCre^{ERT2}* post 32 days tamoxifen injection), NMNAT1 cKO: SARM1 KO (*Nmnat1$^{fl/fl}$: SARM1$^{-/-}$: ActCre^{ERT2}* post 32 days tamoxifen injection). Graphs show the average and error bars represent the standard error. Statistical analysis was performed by two-way ANOVA with Tukey post-hoc test (n = 6 for NMNAT1 WT, n = 2 for NMNAT1 cKO, and n = 7 for NMNAT1 cKO: SARM1 KO). F (8, 108) = 2.6, p = 1.5 x 10^{-3} for scotopic a-wave, F (8, 108) = 1.9, p = 0.032 for scotopic b-wave, F (6, 84) = 3.7, p = 1.7 x 10^{-4} for photopic b-wave. * $P < 0.05$, ** $P < 0.001$ denotes the statistical difference between NMNAT1 WT and NMNAT1 cKO. There is no statistical difference between NMNAT1 WT and NMNAT1 KO: SARM1 KO. (F, G, H)

Quantification of retinal metabolite using LC-MSMS in retinal tissues from NMNAT1 WT (*Nmnat1*$^{fl/fl}$*: Sarm1*$^{+/-}$), NMNAT1 cKO (*Nmnat1*$^{fl/fl}$*: ActCre*^{ERT2} post 32 days tamoxifen injection), NMNAT1 cKO: SARM1 KO (*Nmnat1*$^{fl/fl}$*: SARM1*$^{-/-}$*: ActCre*^{ERT2} post 32 days tamoxifen injection). Graphs show the first and third quartile (box height), median (line in the box), and minimum and maximum (whisker). Statistical analysis was performed by one-way ANOVA with Holm-Bonferroni multiple comparison (n = 3 for NMNAT1 WT, n = 2 for NMNAT1 cKO, and n = 3 for NMNAT1 cKO: SARM1 KO). $F(2, 5) = 7.5$, $p = 0.031$ for NAD^+, $F(2, 5) = 18.7$, $p = 0.0047$ for NMN, and $F(2, 5) = 498.2$, $p = 1.76 \times 10^{-6}$ for cADPR. * $P < 0.05$ denotes the significant statistical difference against NMNAT1 WT. Graphs show the all data points and median (cross bars).

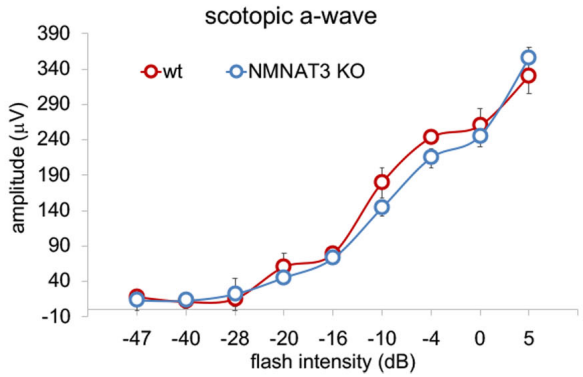

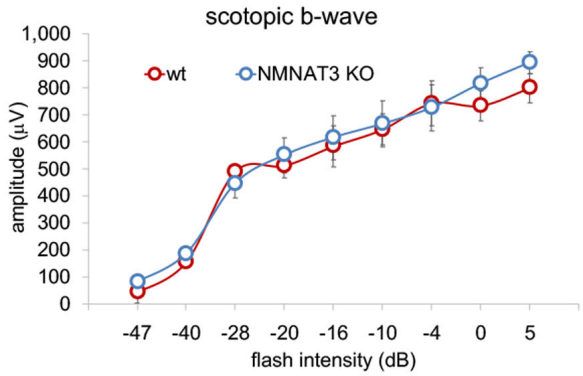

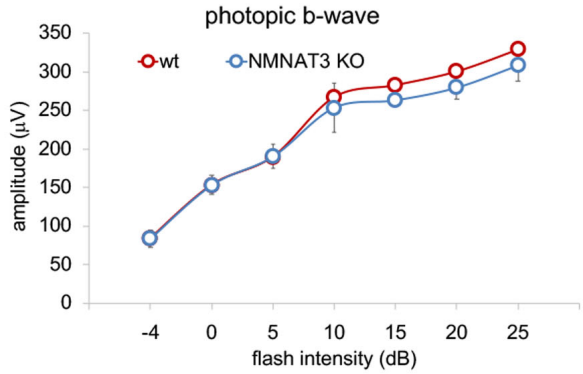

Supplemental Figure1. ERG analysis of NMNAT3-deficient retina. ERG analysis of WT or NMNAT3 knock out mice (NMNAT3 KO). Graphs show the average and error bars represent the standard error. Statistical analysis was performed by one-way ANOVA (n = 3 for WT or NMNAT3 KO). $F(8, 36) = 0.78$, $p = 0.623$ for scotopic a-wave, $F(8, 36) = 0.28$, $p = 0.97$ for scotopic b-wave, $F(6, 28) = 0.23$, $p = 0.97$ for photopic b-wave and there is no statistical difference between WT and NMNAT3 KO in each flush intensity.

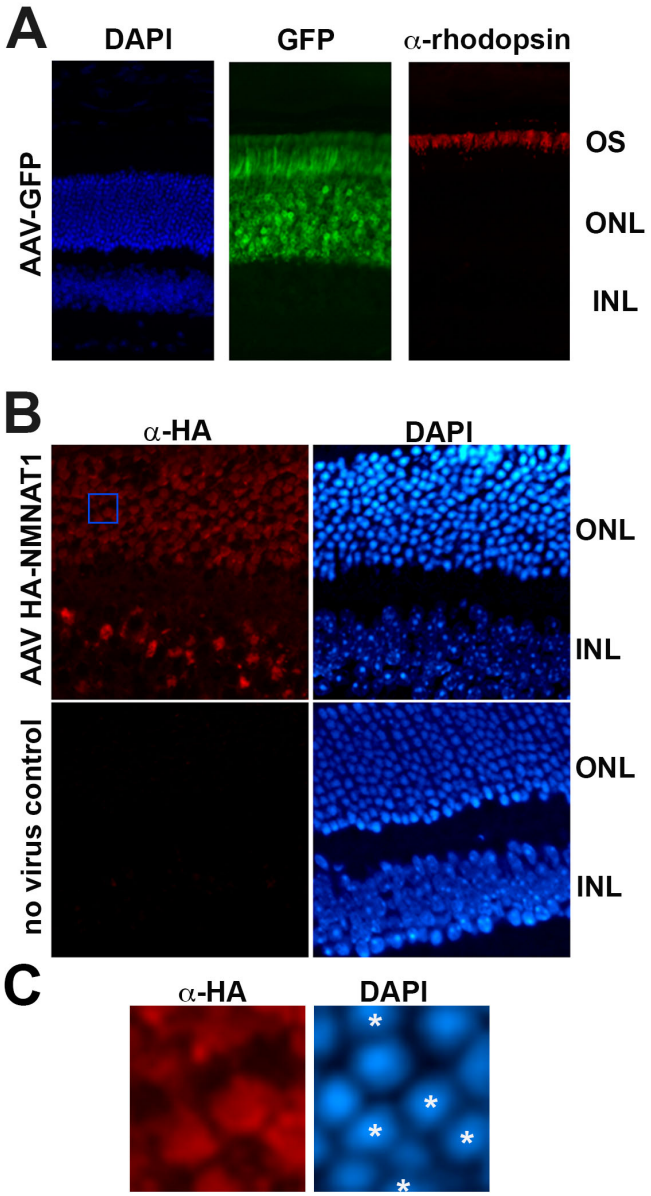

Supplemental Figure2 AAV mediated GFP and NMNAT1 expression in the retina. (A) Fluorescent microscope images of the retina after subretinal injection of AAV expressing GFP. The photoreceptor cell layer is identified with immunostaining with antibody against human rhodopsin. (B, C) Fluorescent microscope images of the retina after subretinal injection of AAV expressing HA-tagged human NMNAT1. The expression of NMNAT1 is shown by immunohistochemistry with antibody against HA epitope tag and nuclei are visualized with DAPI. Asterisks indicate the cells expressing HA-Nmnat1.

Materials and methods

Mouse Animal studies were carried out under approved protocols from animal studies committee at Washington University. NMNAT1 mutant mice (*Nmnat1* $_{FRTgeo;loxP/+}$) which have FRT sites flanking promoterless *LacZ-neomycin phosphotransferase* gene (*beta Geo*) expression cassette located between exon 2 and 3 together with loxP sites flanking exon 3 was obtained from EUCOMM (NMNAT $^{tm1a(EUCOMM)Wtsi}$). This mouse expresses functionally null truncated NMNAT1 (exon 1 and 2) fused to beta Geo. *Nmnat1* $_{FRTgeo;loxP/+}$ heterozygote mice were viable and fertile however, in consistent with former results, no whole body knockout (Nmnat1$_{FRTgeo;loxP/FRTgeo;loxP}$) was born [42]. Next *Nmnat1* $_{FRTgeo;loxP/+}$ mice were crossed with FLP recombinase expressing mice in the C57BL/6 J background to remove beta Geo cassette flanked by FRT sites and RD8 mutation that might affect the ocular phenotypes [66]. The resultant mice (*Nmnat1* $^{fl/+}$) have two loxP sites flanking the third exon. Then *Nmnat1* $^{fl/+}$ mice were crossed with mice expressing inducible Cre recombinase under actin promoter (ActCre^{ERT2}) and *Nmnat1*$^{fl/fl}$*: ActCre*^{ERT2}mice were generated. All genotypes were confirmed by genomic PCR. NMNAT1 whole body knockout mice were generated by injecting 100 μg/g 4-hydroxytamoxifen (Sigma) into 6 to 8 weeks old *Nmnat1*$^{fl/fl}$*:* ActCre^{ERT2} with IP for total 10 days with 2 days rest after first 5 days injection. The last day of injection was counted as day 0 after tamoxifen injection. Mice expressing Cre recombinase (acinCreERT2) were obtained from The Jackson Laboratory. To generate mice lacking *Nmnat1* specifically from rod photoreceptors, we crossed *Nmnat1*$^{fl/fl}$ mice with mice carrying a copy of the Rhodopsin- iCre75 transgene, which were provided by Dr. Ching-Kang Jason Chen [47]. To generate mice lacking NMNAT1 specifically from cone photoreceptors, we crossed *Nmnat1* $_{loxP/loxP}$ mice with mice carrying one copy of the human red/green pigment-Cre (HRGP-Cre) transgene, which were provided by Dr. Yun Le [49]. Vmd2-Cre mice were obtained from Dr. Thomas Ferguson [52]. SARM1 knockout mice were obtained from Dr. Marco Colonna [58]. NMNAT3 knockout mice were derived from ES cells (Nmnat3$^{tm1(KOMP)Mbp}$, Knockout Mouse Project (KOMP)) in our facility and crossed with C57BL/6 J mice for at least five generations.

AAV preparation

Plasmids containing the photoreceptor-specific human rhodopsin kinase (hGRK1) promoter up stream of either GFP or HA-tagged NMNAT1 were packaged in AAV8(Y733F) capsid. The detailed methodology of vector production and purification has been previously described [67]. Briefly, vectors were packaged using a plasmid based system in HEK293 cells by $CaPO_4$ transfection. Cells were harvested and lysed by successive freeze thaw cycles. Virus within the lysate was purified by discontinuous iodixanol step gradients followed by further purification via column chromatography on a 5ml HiTrap Q sepharose column using a Pharmacia AKTA FPLC system (Amersham Biosciences, Piscataway, NJ, USA). Vectors were then concentrated and buffer exchanged into Alcon BSS (Sodium-155.7 mM, Potassium- 10.1 mM, Calcium- 3.3 mM, Magnesium- 1.5 mM, Chloride- 128.9 mM, Citrate- 5.8 mM, Acetate- 28.6 mM, Osmolality- 298 mOsm) supplemented with Tween 20 (0.014%). Virus was titered by qPCR relative to a standard and stored at -80C° as previously described [68].

Subretinal Injections Mice were anesthetized with a mixture of ketamine (70-80 mg/kg) and xylazine (15 mg/kg) injected intraperitoneally. The pupil was dilated with 1% tropicamide and topical anesthesia (0.5% proparacaine hydrochloride ophthalmic solution) was also applied to the eye. A self-sealing scleral incision was made by using the tip of a 31 G needle with the bevel pointed down. Then a 33G needle on a Hamilton syringe was inserted into the scleral incision and 1 ul of AAV containing solutions were injected in the subretinal space inducing a transient retinal detachment. The needle was slowly removed to prevent reflux and an ophthalmic ointment of neomycin/polymyxin B sulfate/bacitracin zinc was applied to the injected eye.

Fundus microscopy and fluorescent angiography Digital color fundus photography was performed using the Micron III retinal imaging system (Phoenix Research Laboratories). Prior to fundus imaging, mice were anesthetized with an intraperitoneal injection of 86.9 mg/kg ketamine and 10 mg/kg xylazine and administered 1.0% tropicamide eye drops (Bausch & Lomb) to dilate the pupils. For in vivo imaging of the retinal vasculature, mice were injected via the femoral vein with 100 μL of 50 mg/mL (5 mg) of 2,000,000 MW FITC conjugated dextran (Sigma-Aldrich). After allowing 5 min for circulation, Goniosoft solution (Ocusoft) was applied

to the eye, and Fitc-Dextran perfusing the retinal fundus was imaged using appropriate filter sets on a MicronIII (Phoenix Research Laboratories) retinal imaging system.

Electroretinography (ERG) ERG was performed as previously described (Hennig et al., 2013) by using the UTAS-E3000 Visual Electrodiagnostic System running EM for Windows (LKC Technologies). Mice were anesthetized by intra peritoneal injection of a mixture of 86.9 mg/kg ketamine and 13.4 mg/kg xylazine. The recording electrode was a platinum loop placed in a drop of methylcellulose on the surface of the cornea; a reference electrode was placed sub-dermally at the vertex of the skull and a ground electrode under the skin of the back or tail. Stimuli were brief white flashes delivered via a Ganzfeld integrating sphere, and signals were recorded with bandpass settings of 0.3 Hz to 500 Hz. After a 10-minute stabilization period, a 9-step scotopic intensity series was recorded that included rod-specific/scotopic bright flash responses. After a 5-minute light adaptation period on a steady white background, a 7-step cone-specific/photopic intensity series was recorded. Scotopic and photopic b-wave amplitudes and scotopic a-wave amplitudes were recorded for all flash intensities. We extracted quantitative measurements from the ERG waveforms using an existing Microsoft Excel macro that defines the a-wave amplitude as the difference between the average pre-trial baseline and the most negative point of the average trace and defines the b-wave amplitude as the difference between this most negative point to the highest positive point, without subtracting oscillatory potentials.

Quantitative RT-PCR Mice were euthanized and eyeballs were enucleated and retinas were dissected and immediately freeze in liquid N_2. On the day of preparation, Trizol was directly added to the frozen retina and tissues were homogenized with Polytron and RNA was extracted using Trizol (Thermo Fisher Scientific) and chloroform (Sigma) phase separation. Quantitative RT-PCR reaction was performed with primers (*Nmnat1*-forward: AGAACTCACACTGGGTGGAAG, *Nmnat1*-reverse: CAGGCTTTTCCAGTGCAGGTG, Gapdh-forward: TGCCCCCATGTTTGTGATG, Gapdh-reverse: TGTGGTCATGAGCCCTTCC with reaction mixture (ThermoFisher, SYBR® Green PCR Master Mix) and monitored with Prism 7900HT (ABI) and analyzed with delta-CT method.

Histology Mice were euthanized and eyeballs were enucleated and fixed in 4% formalin for 8hr then washed with PBS and then embedded in paraffin. The numbers of nuclei in the outer or inner nuclear layer were analyzed using HE stained retinal sections. Outer or inner nuclear layer was visually determined and the number of nucleus in each layer was counted and normalized by the length parallel to each layer of the retina. Data were expressed relative to the total number of nuclei in the WT (Fig. 3B, 4E, 4I, and 5B) or control fellow eyes (Fig. 6B). For immunostaining of the HA epitope tag, paraffin embedded eye sections were deparaffinized and treated with formic acid (70% in water) for 15min at room temperature. Sections were rinsed and treated with blocking solution (goat IgG). Primary antibody against HA (Cell Signaling Technology, 3724, 1:400) and secondary antibody Jackson Immuno Research Laboratories, AlexaFluo@568, 111-585-003) were used to visualize the HA-tagged NMNAT1. Primary antibody against rhodopsin (Abcam, ab3267, 1:500) was used to identify the photoreceptor outer segment. Slides were analyzed under the microscope (Nikon, Eclipse 80i) after the nuclear staining with DAPI and mounting (Vector Laboratories, VECTASHIELD® with DAPI, H-1200-10). For x-gal staining, retina were dissected and fixed in the cold fixation buffer (0.2% Glutaraldehyde, 5mM EGTA, 2mM MgCl2, 0.1M K-phoshate buffer pH7.2) for 1 hr, wash with detergent rinse (0.02% Igepal, 0.01% Sodium Deoxycholate, and 2mM $MgCl_2$in 0.1M phosphate buffer pH 7.3), and incubated with X-Gal solution (1mg/ml X-Gal, 0.02% Igepal, 0.01% Sodium Deoxycholate, 5mM Potassium Ferricyanide, 5mM Pottassium Ferrocyanide, and 2mM $MgCl_2$,0.1M phosphate buffer pH 7.3) for 10 hours in the dark at room temperature. Tissues were rinsed with PBS then fix with 4% PFA for 1 hr then paraffin sections were prepared and the sections were analyzed under the microscope (Nikon, Eclipse 80i).

TUNEL assay The retinal sections were prepared as described above and post-fixed with 4% PFA for 10min and washed in PBS at room temperature. The sections were then exposed to 5μg/ml proteinase K for 5min at room temperature, rinsed once with PBS, fixed in 4%PFA for 10min, and rinse with PBS. Proteinase K treated sections were incubated with terminal deoxynucleotidyl transferase (TdT) buffer containing 1mM $CoCl_2$ (Roche) for 10min at room temperature followed by an incubation with TdT+biotin-16-dUTP solution (containing 2U/μl TdT, 2.5μM biotin-16-dUTP, 1mM $CoCl_2$ in TdT buffer, Roche) for 1h in the humidified chamber at 37℃. Finally, sections were washed with PBS once and incubated with Cy3-

conjugated streptavidin (1:3000; Jackson Immunoresearch) for 1h at room temperature and analyzed under the microscope (Nikon, Eclipse 80i) after nuclear staining with DAP (Vector Laboratories, VECTASHIELD® with DAPI, H-1200-10).

Metabolite measurement Mice were euthanized and eyeballs were enucleated and retinas were dissected and immediately freeze in liquid N_2. On the day of extraction, retinal tissues were homogenized in 160 μl of cold 50% MeOH solution in water using homogenizer (Bransoon) and then centrifuged (15,000 g, 4 ºC, 10min). Clear supernatant was transferred to new tube containing 100 μl chloroform and vigorously shake then centrifuged (15,000 g, 4 ºC, 10min). The chloroform extraction was repeated three times. Clear aqueous phase (120 μl) was transferred to new tube and then lyophilized and stored at -80 ºC until measurement. Lyophilized samples were reconstituted with 60 µl of 5 mM ammonium formate (Sigma) and centrifuged at 12,000 x g for 10 min. Cleared supernatant was transferred to the sample tray. Serial dilutions of standards for each metabolite in 5 mM ammonium formate were used for calibration. Liquid chromatography was performed by HPLC (1290; Agilent) with Atlantis T3 (LC 2.1 x 150 mm, 3 µm; Waters) for steady-state metabolite assays [44]. For steady-state metabolite analysis, 20 μl of samples were injected at a flow rate of 0.15 ml/min with 5 mM ammonium formate for mobile phase A and 100% methanol for mobile phase B. Metabolites were eluted with gradients of 0–10 min, 0–70% B; 10–15 min, 70% B; 16–20 min, 0% B [44]. The metabolites were detected with a triple quadrupole mass spectrometer (6460, Agilent) under positive ESI multiple reaction monitoring (MRM) using m/z for NAD^+:664 > 28, NMN:335 >123, cADPR: 542>428, and Nam:123 > 80. Metabolites were quantified by MassHunter quantitative analysis tool (Agilent) with standard curves and normalized by the protein amount in the sample.

Statistical analysis Sample number (n) was defined as a number of mice or replicates and indicated in the figure legend. Data comparisons were performed using Mann-Whitney U test, Kruskal-Wallis test, one-way ANOVA, or two-way ANOVA using R. F and P values for ANOVA were reported for each comparison in corresponding figure legends. For multiple comparisons, the Holm-Bonferroni multiple comparison or Tukey post-hoc test was used.

Funding

This work was supported by funds from the National Institutes of Health (AG013730 to J.M., NS087632 & CA219866 to J.M. and A.D., EY019287-06 to RSA, and P30 EY02687 to Washington University, Core Grant for Vision Research). The Needleman Center for Neurometabolism and Axonal therapeutics, the Edward N. & Della L. Thome Memorial Foundation Award (RSA); the Carl and Mildred Almen Reeves Foundation (RSA); the Starr Foundation (RSA); the Bill and Emily Kuzma Family Gift for Retinal Research (RSA); the Jeffrey Fort Innovation Fund (RSA); the Glenn Foundation for Medical Research, the Research to Prevent Blindness Nelson Trust Award (RSA); and the Research to Prevent Blindness, Inc, Unrestricted Grant to Washington University School of Medicine Department of Ophthalmology.

Acknowledgements

We thank Amy Strickland, Nina Panchenko, Kimberly Kruse, Andrea Santeford, Rachel McClarney, Simburger Kelli, Neiner Alicia, and Cassidy Menendez for technical assistance.

Competing interests

J.M. and A. D. co-founders and shareholders in Disarm Therapeutics. Y.S. is a consultant to Disarm Therapeutics.

1. Falk, M. J. *et al.* NMNAT1 mutations cause Leber congenital amaurosis. *Nat. Genet.* **44,** 1040–1045 (2012).
2. Perrault, I. *et al.* Mutations in NMNAT1 cause Leber congenital amaurosis with early-onset severe macular and optic atrophy. *Nat. Genet.* **44,** 975–977 (2012).
3. Koenekoop, R. K. *et al.* Mutations in NMNAT1 cause Leber congenital amaurosis and identify a new disease pathway for retinal degeneration. *Nat. Genet.* **44,** 1035–1039 (2012).
4. Chiang, P.-W. *et al.* Exome sequencing identifies NMNAT1 mutations as a cause of Leber congenital amaurosis. *Nat. Genet.* **44,** 972–974 (2012).
5. Coppieters, F. *et al.* Hidden Genetic Variation in LCA9-Associated Congenital Blindness Explained by 5'UTR Mutations and Copy-Number Variations of NMNAT1. *Hum. Mutat.* **36,** 1188–1196 (2015).

6. Khan, A. O. *et al.* Genome-wide linkage and sequence analysis challenge CCDC66 as a human retinal dystrophy candidate gene and support a distinct NMNAT1-related fundus phenotype. *Clin. Genet.* **93,** 149–154 (2018).
7. Sasaki, Y., Margolin, Z., Borgo, B., Havranek, J. J. & Milbrandt, J. Characterization of Leber Congenital Amaurosis-associated NMNAT1 Mutants. *J. Biol. Chem.* **290,** 17228–17238 (2015).
8. Zabka, T. S. *et al.* Retinal toxicity, in vivo and in vitro, associated with inhibition of nicotinamide phosphoribosyltransferase. *Toxicol. Sci.* **144,** 163–172 (2015).
9. Lin, J. B. *et al.* NAMPT-Mediated NAD+ Biosynthesis Is Essential for Vision In Mice. *Cell Reports* **17,** 69–85 (2016).
10. Zhu, Y., Zhang, L., Sasaki, Y., Milbrandt, J. & Gidday, J. M. Protection of mouse retinal ganglion cell axons and soma from glaucomatous and ischemic injury by cytoplasmic overexpression of Nmnat1. *Invest. Ophthalmol. Vis. Sci.* **54,** 25–36 (2013).
11. Eblimit, A. *et al.* NMNAT1 E257K variant, associated with Leber Congenital Amaurosis (LCA9), causes a mild retinal degeneration phenotype. *Exp. Eye Res.* **173,** 32–43 (2018).
12. Wang, X., Fang, Y., Liao, R. & Wang, T. Targeted deletion of Nmnat1 in mouse retina leads to early severe retinal dystrophy. *bioRxiv* 210757 (2017). doi:10.1101/210757
13. Siemiatkowska, A. M. *et al.* Nonpenetrance of the most frequent autosomal recessive leber congenital amaurosis mutation in NMNAT1. *JAMA Ophthalmol* **132,** 1002–1004 (2014).
14. Greenwald, S. H. *et al.* Mouse Models of NMNAT1-Leber Congenital Amaurosis (LCA9) Recapitulate Key Features of the Human Disease. *Am. J. Pathol.* **186,** 1925–1938 (2016).
15. Kuribayashi, H. *et al.* Roles of Nmnat1 in the survival of retinal progenitors through the regulation of pro-apoptotic gene expression via histone acetylation. *Cell Death Dis* **9,** 891–14 (2018).
16. Zhai, R. G. *et al.* Drosophila NMNAT maintains neural integrity independent of its NAD synthesis activity. *PLoS Biol.* **4,** e416 (2006).
17. Zhai, R. G. *et al.* NAD synthase NMNAT acts as a chaperone to protect against neurodegeneration. *Nature* **452,** 887–891 (2008).
18. Schuster, A. *et al.* The phenotype of early-onset retinal degeneration in persons with RDH12 mutations. *Invest. Ophthalmol. Vis. Sci.* **48,** 1824–1831 (2007).
19. Kennan, A. *et al.* Identification of an IMPDH1 mutation in autosomal dominant retinitis pigmentosa (RP10) revealed following comparative microarray analysis of transcripts derived from retinas of wild-type and Rho(-/-) mice. *Hum. Mol. Genet.* **11,** 547–557 (2002).
20. Bowne, S. J. *et al.* Mutations in the inosine monophosphate dehydrogenase 1 gene (IMPDH1) cause the RP10 form of autosomal dominant retinitis pigmentosa. *Hum. Mol. Genet.* **11,** 559–568 (2002).
21. Lin, J. B., Lin, J. B., Chen, H. C., Chen, T. & Apte, R. S. Combined SIRT3 and SIRT5 deletion is associated with inner retinal dysfunction in a mouse model of type 1 diabetes. *Scientific Reports 2016 6* **9,** 3799–12 (2019).
22. Lin, J. B. & Apte, R. S. NAD+ and sirtuins in retinal degenerative diseases: A look at future therapies. *Prog Retin Eye Res* **67,** 118–129 (2018).
23. Verdin, E. NAD+ in aging, metabolism, and neurodegeneration. *Science* **350,** 1208–1213 (2015).
24. Berger, F., Lau, C., Dahlmann, M. & Ziegler, M. Subcellular compartmentation and differential catalytic properties of the three human nicotinamide mononucleotide adenylyltransferase isoforms. *J. Biol. Chem.* **280,** 36334–36341 (2005).
25. Walker, L. J. *et al.* MAPK signaling promotes axonal degeneration by speeding the turnover of the axonal maintenance factor NMNAT2. *Elife* **6,** 545 (2017).

26. Sasaki, Y., Vohra, B. P. S., Baloh, R. H. & Milbrandt, J. Transgenic mice expressing the Nmnat1 protein manifest robust delay in axonal degeneration in vivo. *J. Neurosci.* **29,** 6526–6534 (2009).
27. Babetto, E. *et al.* Targeting NMNAT1 to axons and synapses transforms its neuroprotective potency in vivo. *J. Neurosci.* **30,** 13291–13304 (2010).
28. Gilley, J. & Coleman, M. P. Endogenous Nmnat2 Is an Essential Survival Factor for Maintenance of Healthy Axons. *PLoS Biol.* **8,** e1000300 (2010).
29. Gerdts, J., Brace, E. J., Sasaki, Y., DiAntonio, A. & Milbrandt, J. SARM1 activation triggers axon degeneration locally via NAD^+ destruction. *Science* **348,** 453–457 (2015).
30. Sasaki, Y., Nakagawa, T., Mao, X., DiAntonio, A. & Milbrandt, J. NMNAT1 inhibits axon degeneration via blockade of SARM1-mediated NAD+depletion. *Elife* **5,** 1010 (2016).
31. Gilley, J., Orsomando, G., Nascimento-Ferreira, I. & Coleman, M. P. Absence of SARM1 rescues development and survival of NMNAT2-deficient axons. *Cell Reports* **10,** 1974–1981 (2015).
32. Figley, M. D. & DiAntonio, A. The SARM1 axon degeneration pathway: control of the NAD+ metabolome regulates axon survival in health and disease. *Current Opinion in Neurobiology* **63,** 59–66 (2020).
33. Russell, S. *et al.* Efficacy and safety of voretigene neparvovec (AAV2-hRPE65v2) in patients with RPE65-mediated inherited retinal dystrophy: a randomised, controlled, open-label, phase 3 trial. *Lancet* **390,** 849–860 (2017).
34. Gardiner, K. L. *et al.* Long-Term Structural Outcomes of Late-Stage RPE65 Gene Therapy. *Mol. Ther.* **28,** 266–278 (2020).
35. Apte, R. S. Gene Therapy for Retinal Degeneration. *Cell* **173,** 5 (2018).
36. Auricchio, A., Smith, A. J. & Ali, R. R. The Future Looks Brighter After 25 Years of Retinal Gene Therapy. *Hum. Gene Ther.* **28,** 982–987 (2017).
37. Kay, C. N. *et al.* Targeting photoreceptors via intravitreal delivery using novel, capsid-mutated AAV vectors. *PLOS ONE* **8,** e62097 (2013).
38. Boye, S. L. *et al.* AAV-mediated gene therapy in the guanylate cyclase (RetGC1/RetGC2) double knockout mouse model of Leber congenital amaurosis. *Hum. Gene Ther.* **24,** 189–202 (2013).
39. Sasaki, Y. *et al.* cADPR is a gene dosage-sensitive biomarker of SARM1 activity in healthy, compromised, and degenerating axons. *Experimental Neurology* **329,** 113252 (2020).
40. DiAntonio, A. Axon degeneration: mechanistic insights lead to therapeutic opportunities for the prevention and treatment of peripheral neuropathy. *Pain* **160 Suppl 1,** S17–S22 (2019).
41. Krauss, R., Bosanac, T., Devraj, R., Engber, T. & Hughes, R. O. Axons Matter: The Promise of Treating Neurodegenerative Disorders by Targeting SARM1-Mediated Axonal Degeneration. *Trends Pharmacol. Sci.* **41,** 281–293 (2020).
42. Conforti, L. *et al.* Reducing expression of NAD+ synthesizing enzyme NMNAT1 does not affect the rate of Wallerian degeneration. *FEBS J.* **278,** 2666–2679 (2011).
43. Slivicki, R. A., Ali, Y. O., Lu, H.-C. & Hohmann, A. G. Impact of Genetic Reduction of NMNAT2 on Chemotherapy-Induced Losses in Cell Viability In Vitro and Peripheral Neuropathy In Vivo. *PLOS ONE* **11,** e0147620 (2016).
44. Hikosaka, K. *et al.* Deficiency of nicotinamide mononucleotide adenylyltransferase 3 (nmnat3) causes hemolytic anemia by altering the glycolytic flow in mature erythrocytes. *J. Biol. Chem.* **289,** 14796–14811 (2014).
45. Eells, J. T. Mitochondrial Dysfunction in the Aging Retina. *Biology (Basel)* **8,** 31 (2019).
46. Ferrington, D. A., Fisher, C. R. & Kowluru, R. A. Mitochondrial Defects Drive Degenerative Retinal Diseases. *Trends Mol Med* **26,** 105–118 (2020).

47. Li, S. *et al.* Rhodopsin-iCre transgenic mouse line for Cre-mediated rod-specific gene targeting. *Genesis* **41,** 73–80 (2005).
48. Aït-Ali, N. *et al.* Rod-derived cone viability factor promotes cone survival by stimulating aerobic glycolysis. *Cell* **161,** 817–832 (2015).
49. Le, Y.-Z. *et al.* Targeted expression of Cre recombinase to cone photoreceptors in transgenic mice. *Mol. Vis.* **10,** 1011–1018 (2004).
50. Nakamura, M., Skalet, J. & Miyake, Y. RDH5 gene mutations and electroretinogram in fundus albipunctatus with or without macular dystrophy: RDH5 mutations and ERG in fundus albipunctatus. *Doc Ophthalmol* **107,** 3–11 (2003).
51. van Soest, S., Westerveld, A., de Jong, P. T., Bleeker-Wagemakers, E. M. & Bergen, A. A. Retinitis pigmentosa: defined from a molecular point of view. *Surv Ophthalmol* **43,** 321–334 (1999).
52. Esumi, N., Oshima, Y., Li, Y., Campochiaro, P. A. & Zack, D. J. Analysis of the VMD2 promoter and implication of E-box binding factors in its regulation. *J. Biol. Chem.* **279,** 19064–19073 (2004).
53. Di Stefano, M. *et al.* A rise in NAD precursor nicotinamide mononucleotide (NMN) after injury promotes axon degeneration. *Cell Death and Differentiation 2014 22:5* **22,** 731–742 (2015).
54. Zhao, Z. Y. *et al.* A Cell-Permeant Mimetic of NMN Activates SARM1 to Produce Cyclic ADP-Ribose and Induce Non-apoptotic Cell Death. *iScience* **15,** 452–466 (2019).
55. Datta, P. *et al.* Accumulation of non-outer segment proteins in the outer segment underlies photoreceptor degeneration in Bardet-Biedl syndrome. *Proc. Natl. Acad. Sci. U.S.A.* **112,** E4400–9 (2015).
56. Zhao, L. *et al.* Integrative subcellular proteomic analysis allows accurate prediction of human disease-causing genes. *Genome Res.* **26,** 660–669 (2016).
57. Menon, M. *et al.* Single-cell transcriptomic atlas of the human retina identifies cell types associated with age-related macular degeneration. *Nat Commun* **10,** 4902–9 (2019).
58. Szretter, K. J. *et al.* The immune adaptor molecule SARM modulates tumor necrosis factor alpha production and microglia activation in the brainstem and restricts West Nile Virus pathogenesis. *J. Virol.* **83,** 9329–9338 (2009).
59. Coleman, M. P. & Höke, A. Programmed axon degeneration: from mouse to mechanism to medicine. *Nature Reviews Neuroscience 2011 12:8* **21,** 183–196 (2020).
60. Maeda, A., Golczak, M., Maeda, T. & Palczewski, K. Limited roles of Rdh8, Rdh12, and Abca4 in all-trans-retinal clearance in mouse retina. *Invest. Ophthalmol. Vis. Sci.* **50,** 5435–5443 (2009).
61. Lukowski, S. W. *et al.* A single-cell transcriptome atlas of the adult human retina. *The EMBO Journal* **38,** e100811 (2019).
62. Molday, L. L., Wu, W. W. H. & Molday, R. S. Retinoschisin (RS1), the protein encoded by the X-linked retinoschisis gene, is anchored to the surface of retinal photoreceptor and bipolar cells through its interactions with a Na/K ATPase-SARM1 complex. *J. Biol. Chem.* **282,** 32792–32801 (2007).
63. Ozaki, E. *et al.* SARM1 deficiency promotes rod and cone photoreceptor cell survival in a model of retinal degeneration. *Life Sci Alliance* **3,** e201900618 (2020).
64. Geisler, S. *et al.* Gene therapy targeting SARM1 blocks pathological axon degeneration in mice. *J. Exp. Med.* **216,** 294–303 (2019).
65. Ko, K. W., Milbrandt, J. & DiAntonio, A. SARM1 acts downstream of neuroinflammatory and necroptotic signaling to induce axon degeneration. *JCB* doi10.1083/jcb.201912047.

66. Mattapallil, M. J. *et al.* The Rd8 mutation of the Crb1 gene is present in vendor lines of C57BL/6N mice and embryonic stem cells, and confounds ocular induced mutant phenotypes. *Invest. Ophthalmol. Vis. Sci.* **53,** 2921–2927 (2012).
67. Zolotukhin, S. *et al.* Production and purification of serotype 1, 2, and 5 recombinant adeno-associated viral vectors. *Methods* **28,** 158–167 (2002).
68. Jacobson, S. G. *et al.* Safety of recombinant adeno-associated virus type 2-RPE65 vector delivered by ocular subretinal injection. *Mol. Ther.* **13,** 1074–1084 (2006).